Journal of Medicinal Chemistry

pubs.acs.org/jmc

Article

Synthesis of the Potent, Selective, and Efficacious β-Secretase (BACE1) Inhibitor NB-360

Heinrich Rueeger, Rainer Lueoend, Rainer Machauer,* Siem J. Veenstra, Philipp Holzer, Konstanze Hurth, Markus Voegtle, Mathias Frederiksen, Jean-Michel Rondeau, Marina Tintelnot-Blomley, Laura H. Jacobson, Matthias Staufenbiel, Grit Laue, and Ulf Neumann

Cite This: J. Med. Chem. 2021, 64, 4677−4696

Read Online

ACCESS | Metrics & More | Article Recommendations | Supporting Information

ABSTRACT: Starting from lead compound **4**, the 1,4-oxazine headgroup was optimized to improve potency and brain penetration. Focusing at the 6-position of the 5-amino-1,4-oxazine, the insertion of a Me and a CF_3 group delivered an excellent pharmacological profile with a pK_a of 7.1 and a very low P-gp efflux ratio enabling high central nervous system (CNS) penetration and exposure. Various synthetic routes to access BACE1 inhibitors bearing a 5-amino-6-methyl-6-(trifluoromethyl)-1,4-oxazine headgroup were investigated. Subsequent optimization of the P3 fragment provided the highly potent *N*-(3-((3*R*,6*R*)-5-amino-3,6-dimethyl-6-(trifluoromethyl)-3,6-dihydro-2*H*-1,4-oxazin-3-yl)-4-fluorophenyl)-5-cyano-3-methylpicolinamide **54** (**NB-360**), able to reduce significantly Aβ levels in mice, rats, and dogs in acute and chronic treatment regimens.

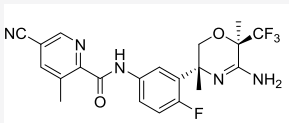

54 (NB-360)

BACE1 IC_{50}	5 nM
wtAPP-CHO cell IC_{50}	3 nM
pK_a	7.1
MDR1-MDCK efflux ratio	1.9

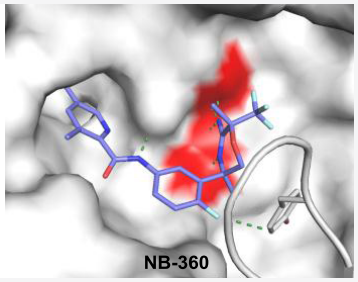

INTRODUCTION

Alzheimer's disease (AD) is the world's leading cause of dementia and the most prevalent neurodegenerative disease. AD currently constitutes a considerable unmet medical need and is expected to become a major challenge for the healthcare systems of both industrial and developing countries during the coming decades. Accumulation of amyloid-β (Aβ) in parenchymal plaques and the brain vasculature and hyperphosphorylated tau in neurofibrillary tangles is a pathological hallmark of the disease.[1] Neuroinflammation, driven by plaque-activated microglia and astrocytes, is a likely mediator between amyloid pathology and synaptic and neuronal dysfunction and neuron loss.[2] Currently available longitudinal data suggest that abnormal deposition of Aβ starts about two decades before the onset of clinical disease, while markers of neurodegeneration (elevated tau protein in cerebrospinal fluid (CSF)) can be detected several years before dementia diagnosis.[3−5] Progress to identify patients with elevated AD risk in the presymptomatic stage has fueled therapeutic concepts that aim to start antiamyloid treatments already in the "preclinical" (only Aβ pathology present) or the "prodromal" (Aβ pathology plus signs of early neurodegeneration) stage of the disease.[6] First clinical data indicating improved efficacy of the Aβ antibody solenazumab in patients with early, compared to advanced, AD further support the current ideas of preventive treatment.[7]

Aβ is generated in the β-secretase pathway from the large transmembrane β-amyloid precursor protein (APP). The membrane-bound aspartic protease BACE1 (EC 3.4.23.46) initiates the pathway by cleaving APP at position one of Aβ, generating the secreted amino-terminal part of APP (sAPPβ) as well as the carboxy-terminal fragment C99. This transmembrane fragment is further cleaved by γ-secretase leading to Aβ. Alternatively, APP may also be processed *via* the non-amyloidogenic pathway, which is initiated by the metalloprotease α-secretase, which cleaves in the center of Aβ leading to sAPPα and C83.[8,9]

Knock out of the BACE1 gene blocks the generation of Aβ and C99, shifting the APP processing toward the α-secretase pathway as indicated by an increase in sAPPα and C83.[10] Interestingly, mice carrying only a single BACE1 allele showed a 50% reduction in BACE1 enzyme activity but a much smaller effect on Aβ.[11] Nevertheless, a moderate 12% Aβ decrease in transgenic mice carrying a single BACE1 allele translated into a pronounced (70−90%) long-term reduction of Aβ deposition.[12]

BACE2 is a closely related protein, with high similarity in sequence and three-dimensional structure, and its physiological role is not well understood.[13] Current BACE1 inhibitors show little or no selectivity over BACE2, and it was unknown

Received: December 11, 2020
Published: April 12, 2021

Table 1. Examples of Early Disclosed BACE1 Inhibitors with Amidine Headgroups[e]

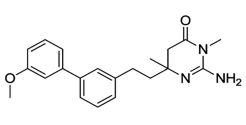
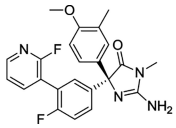
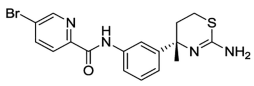

	1[c]	2[d]	3[e]
hBACE1 IC_{50} [μM][a]	0.49	0.033	0.044
APP CHO IC_{50} [μM][a]	0.48	0.122	0.004
pK_a	9.5	6.6	8.8
ER[b]	25	59	6.1

[a]Values are means of at least three experiments. [b]ER is the efflux ratio (P_{BL-AP}/P_{AP-BL}) in MDCK cells transfected with human MDR1. [c]Ref 35. [d]Ref 36. [e]Ref 37.

whether such lack of selectivity would have consequences in chronic pharmacological treatment. BACE1 has a number of physiological substrates in addition to APP. Germ-line deletion of the BACE1 gene affected the processing of neuregulin1 (NRG1), resulting in hypomyelination,[14,15] APP-like protein1 and 2 (APLP1/2),[16] the close homologue of L1 (CHL1),[17] seizure-6-protein (SEZ6),[18] and others. Nonetheless, general and consistent malfunction and sickness were not observed in mice lacking BACE1 activity. Thus, it seems necessary to elucidate in detail the relative importance of these BACE1 substrates during embryonal development and adult life. Moreover, it was shown that some BACE1 physiological substrates are processed in the trans Golgi network, while APP is primarily cleaved in the more acidic endosomal compartment. The intracellular inhibitor distribution may therefore contribute to the effects on different BACE1 substrates. While our understanding of BACE1 biology continues to evolve, careful monitoring of the safety of BACE1 inhibitors during clinical trials is critical. Recent clinical data show that strong pharmacological inhibition of BACE1 is accompanied by signs of worsening in some cognitive domains.[19] Therefore, safety and efficacy of doses leading to partial BACE1 inhibition need to be investigated carefully.

BACE1 belongs to the aspartyl protease family with two aspartic acids constituting the catalytic dyad in the center of a large binding site extending over 6−8 substrate amino acid residues. Standard high-throughput screening (HTS) methods failed in many institutions to deliver suitable hits. Therefore, the initial phase of the BACE1 inhibitor design was dominated by peptidomimetic approaches, similar to those used for inhibitors of renin and HIV protease. These efforts produced potent inhibitors, which lacked significant brain penetration and *in vivo* CNS Aβ lowering activity at pharmacological doses.[20,21] Consequently, the focus shifted to nonpeptidic BACE1 inhibitors with physicochemical properties within the CNS drug space. During lead optimization, special attention has to be paid to the blood−brain barrier (BBB) penetration capability, as well as cellular activity and metabolic stability.[22,23] A moderate-to-high permeability (>50−150 nm/s) and minimal P-glycoprotein (P-gp) efflux (efflux/flux ratio (ER) less than 3-fold) in the MDCK-MDR1 assay have to be attained to achieve a good BBB penetration and is commonly observed for CNS drugs.[24−27] Remaining within the boundaries of the CNS drug property space during the structure-based design (MW < 450 Da, PSA < 70 Å, clog P < 4, HBD < 2, number of oxygen and nitrogen atoms $\sum$(N + O) < 5 and pK_a < 8 to minimize P-gp[28−31] and hERG channel[32] interactions) should lead to drug candidates with acceptable pharmacokinetics, brain exposure, and cardiosafety profiles. By considering these constraints in the design of cyclic hydroxyethylamine BACE1 inhibitors, we could demonstrate brain exposure but were unable to overcome the high metabolic clearance observed in the cyclic sulfone and cyclic sulfoxide hydroxyethylamine scaffolds.[33,34]

A key advancement in the BACE1 inhibitor design was the discovery of amidine- or guanidine-containing heterocycles by high-throughput or/and fragment-based screening.[35−38] An amidine embedded in a cyclic framework, which can form an optimal hydrogen-bonding network with both active site aspartyl moieties, was combined with ideal substitution vectors, derived from structural knowledge gained by X-ray crystallography and molecular modeling.

This has led to a series of BACE1 inhibitors with high potency and ligand efficiency. Selective substitution of the amidine containing cyclic framework with moieties having a low P-gp interaction potential and the capability to reduce the pK_a to ∼7 has provided *in vivo* efficacious BACE1 inhibitors. Several compounds with slightly different substituted cyclic amidine headgroups with such a profile have advanced into clinical studies.[39−46]

Previously, various groups had disclosed frontrunner BACE1 inhibitors containing amidine headgroups (**1**−**3**, Table 1).[35−37] Compound **3**, bearing an amino-thiazine headgroup, an aryl moiety in P1, and an extension into P3 *via* an amide linker, expanded the field beyond 5- and 6-membered acylguanidines **1**−**2** (nomenclature P1, P2, and P3 according to Schechter and Berger[47]) while, at the same time, showing excellent cellular activity and a low efflux ratio (ER) compared to the amino-dihydropyrimidinone (**1**) and amino-hydantoin headgroup (**2**) containing inhibitors.

To assist in the design of novel 6-membered heterocyclic amidine headgroups, we co-crystallized compound **3** with BACE1. In Figure 1, the topology of the active site of BACE1 bound to **3** is highlighted. Tight hydrogen bonds are formed between the protonated 2-amino-thiazine headgroup and the catalytic aspartates Asp32 (2.7 and 2.9 Å) and Asp228 (2.8 and 3.0 Å). In addition, the amide N−H forms a hydrogen bond with the backbone carbonyl of Gly230. The connecting phenyl ring is engaged in a network of van der Waals contacts with hydrophobic residues lining the S1 pocket (Ile118, Trp115, Phe108, and Tyr71 of the enzyme flap). The orientation of the 2-acyl-pyridine moiety projecting into the S3 pocket is stabilized by a favorable intramolecular electrostatic interaction between the NH of the amide bond and the pyridyl nitrogen. An sp^2 nitrogen at this position is preferred over an sp^2 carbon atom to minimize steric interaction with the backbone of

https://doi.org/10.1021/acs.jmedchem.0c02143
J. Med. Chem. 2021, 64, 4677−4696

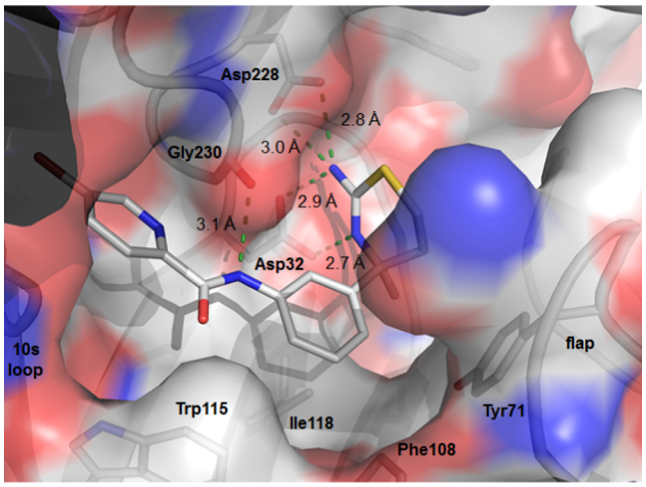

Figure 1. Co-crystal structure of 2-amino-1,3-thiazine inhibitor **3** bound to human BACE1 (PDB ID: 7B1E).

Gly230. This bisarylamide has become a widely used fragment, especially in substituted 6-membered heterocyclic amidine BACE1 inhibitors, likely because of its optimal shape complementary with the S1 and S3 pockets and its discrimination against cathepsin D.[42,43,45,48−50]

Based on the understanding of the binding mode of the 2-amino-1,3-thiazine **3**, the interactions of novel 6-membered amidine heterocycles were assessed together with their potential BBB penetration properties. From this evaluation, we selected the 5-amino-1,4-oxazine headgroup as our starting point.[51] The measured pK_a value of the 6-unsubstituted 5-amino-1,4-oxazine headgroup turned out to be too basic and outside of the target range (Table 2). Therefore, subsequent fine-tuning with different electron-withdrawing substituents at the 6- and/or 3-position was envisioned. Even weak electron-withdrawing substituents at these proximal positions would be expected to have a considerable pK_a lowering effect. In addition, steric shielding of the amidine headgroup was postulated to have a positive impact on activity and permeation by reduced solvation (Figure 2). Additional steric bulk at the 6-position was hypothesized to further increase the chemical and metabolic stability of the 5-amino-1,4-oxazine headgroup. Following this strategy, we were able to generate a series of potent BACE1 inhibitors with druglike properties.

To set the baseline for potency and physicochemical properties of this new class of 5-amino-1,4-oxazine inhibitors, the C6-unsubstituted prototype compound **4** was synthesized.[51] At that time, the predictive power of our internal computational tools for pK_a values was not very strong and a large difference between the calculated and experimentally measured pK_a was observed (6.2 vs 9.5, Table 2). To reduce the amidine pK_a to about 7, we favored small fluoroalkyl substitutions (CF_3, CHF_2, CH_2F) over polar substituents.[51] The introduction of hydroxy, alkoxy, amino, amido, sulfone, and sulfonamide groups was assumed to bear the risk to increase P-gp-mediated efflux due to the increase in polarity (HBD > 2, number of oxygen and nitrogen atoms $\sum$(N + O) > 5). For estimation of the required fluorination level of a methyl group at C6, we tried to transfer pK_a shifts previously described in the literature. The established pK_a shifts of fluoroalkyl groups on amines (ΔpK_a $NHCH_2CH2\mathbf{CH_3}$ to $NHCH_2CH_2\mathbf{CF_3}$ −2.0) have been investigated,[52] which suggested the CF_3 group to be a good option to lower the amidine pK_a to around neutrality. Herein, we disclose our efforts to convert our initial 5-amino-1,4-oxazine lead compound **4** into the 5-amino-6-methyl-6-trifluoromethyl-1,4-oxazine containing inhibitors, a class of compounds (**A**, Figure 2) with an improved physicochemical property profile (measured pK_a ∼ 7 and low efflux ratio) resulting in a robust oral effect in CNS Aβ lowering activity. Related approaches were also pursued by others.[39,42,53] We present here, in more detail, the synthetic access to this highly substituted 5-amino-1,4-oxazine headgroup and structure−activity relationship (SAR) of P3 modifications (**64a−j**).[54] A detailed account of the pharmacokinetic properties and the pharmacological activity of **54** (**NB-360**) in preclinical studies has already been published elsewhere.[55]

CHEMISTRY

Our retrosynthetic analysis is presented in Figure 3. An obvious disconnection for the C6-unsubstituted 5-amino-1,4-oxazine headgroup in **4** was to build the more accessible 1,6-ether linkage in the 1,4-oxazine scaffold from the corresponding *N*-chloroacetylated intermediate prepared from amino alcohol **B** (Path A). The final target compounds could then arise *via* amidine formation from the lactam and generation of the aniline for amide coupling with different P3 fragments. The same disconnection (Path A) for the 3,3,6,6-*tetra*-substituted

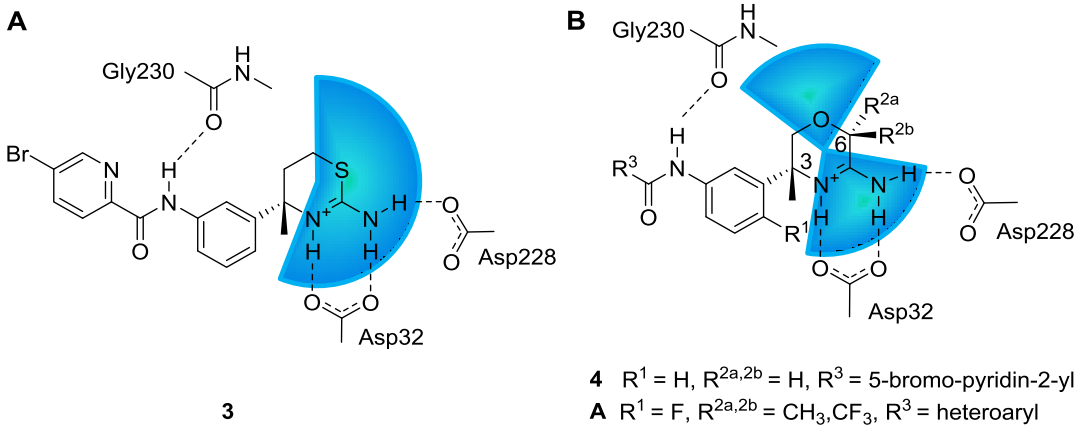

Figure 2. (A) Binding mode of 2-amino-1,3-thiazine **3** and (B) proposed binding mode of 5-amino-1,4-oxazine inhibitors **4** and compound series **A**. Not shielded areas (in blue) decrease with increasing bulk at position 6.

https://doi.org/10.1021/acs.jmedchem.0c02143
J. Med. Chem. 2021, 64, 4677−4696

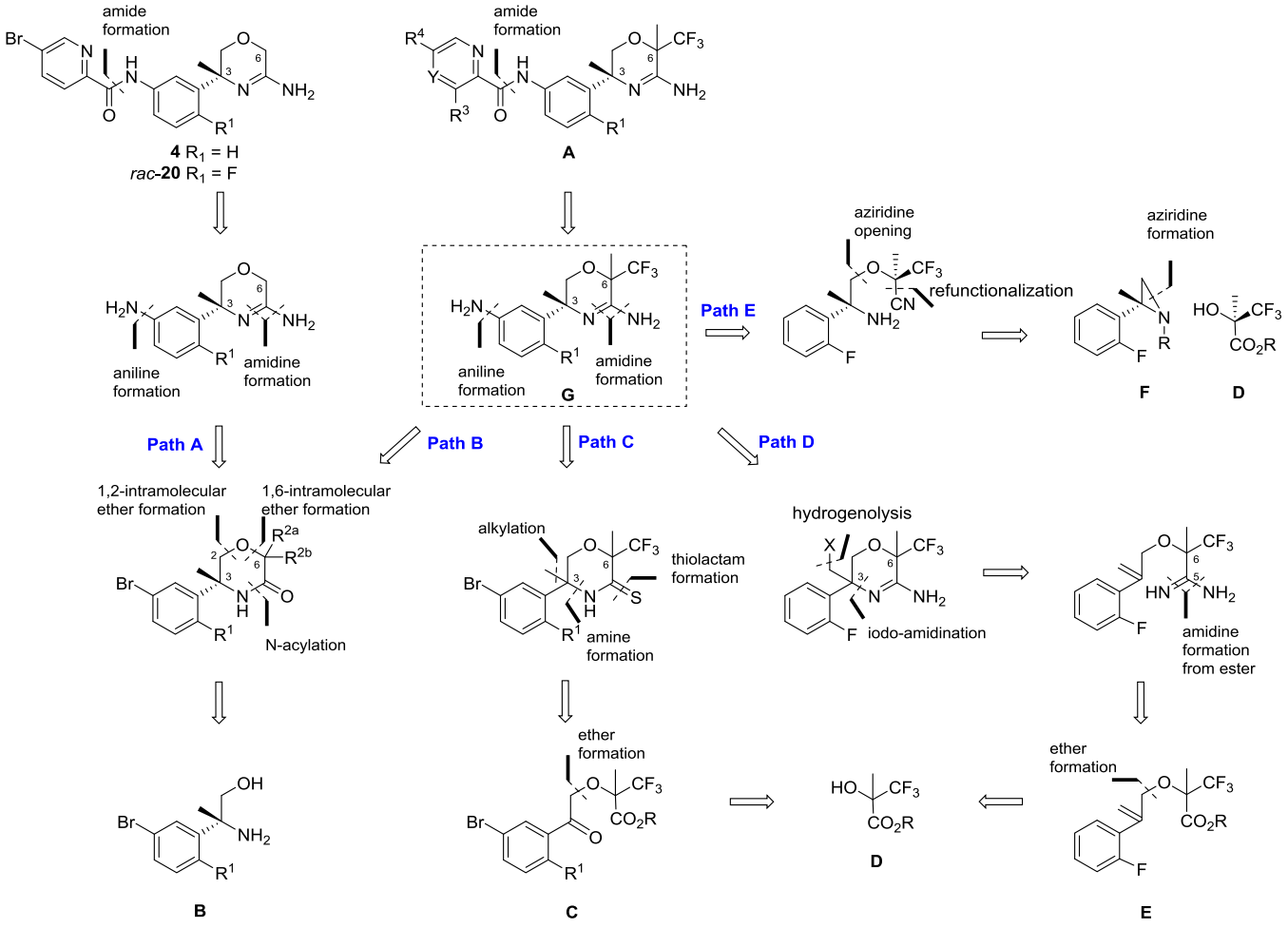

Figure 3. Retrosynthetic analysis of **4**, *rac*-**20**, and compound series **A**.

Scheme 1. Preparation of 4 and *rac*-20—Referring to Retrosynthetic Pathway A[a]

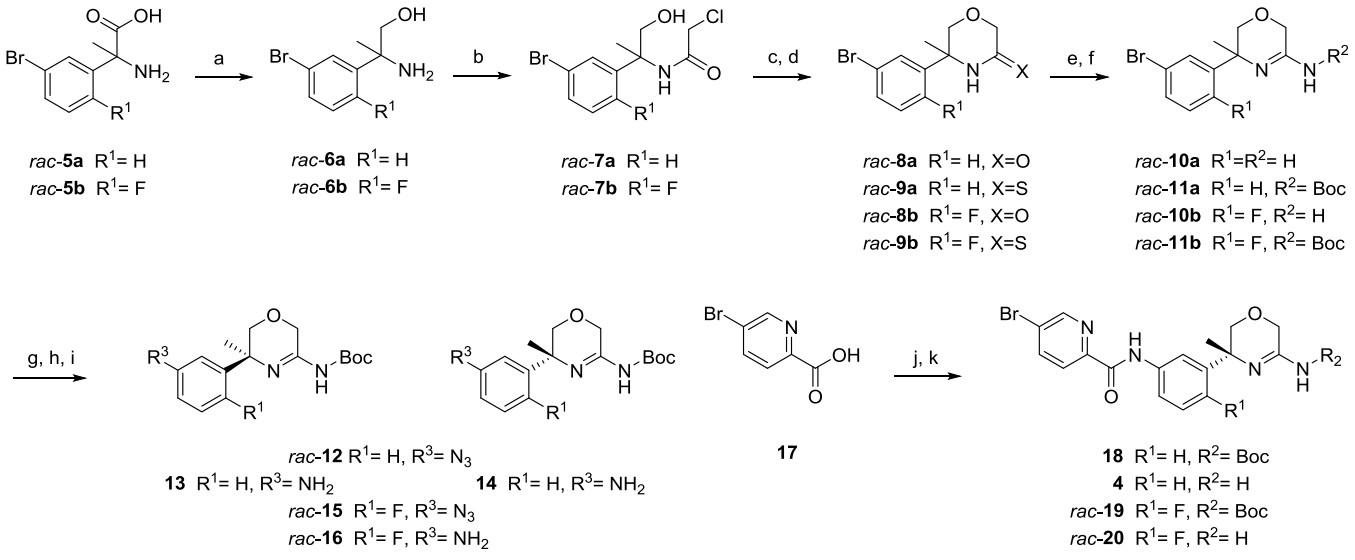

[a]Reagents and conditions: (a) $NaBH_4$, BF_3-Et_2O, tetrahydrofuran (THF), 0−25 °C, 81/84%; (b) chloroacetyl chloride, Na_2CO_3, CH_2Cl_2-H_2O, 0−25 °C, 95/38%; (c) *t*-BuOK, *t*-BuOH, reflux, 32/52%; (d) Lawesson's reagent, THF, reflux, 78/59%; (e) *t*-BuOOH, 7 N NH_3 in MeOH, NH_3 conc., THF, 25 °C, 50/90%; (f) $(Boc)_2O$, *N*,*N*-diisopropylethylamine, CH_2Cl_2, 25 °C, 93/49%; (g) NaN_3, CuI, (1*R*,2*R*)-*N*1,*N*2-dimethylcyclohexane-1,2-diamine, Na-ascorbate, EtOH-H_2O, 90 °C, 51/54%; (h) H_2, Lindlar catalyst, EtOAc, 25 °C, 99/94%; (i) Chiralpak IA 250 mm × 4.6 mm, hexane/EtOH/MeOH 80:10:10, 1.5 mL/min, 39/41%; (j) **17**, EDC, HOAt, *N*,*N*-diisopropylethylamine, *N*,*N*-dimethylformamide (DMF), 25 °C, 93/79%; (k) 4 N HCl in dioxane, 25−40 °C, 99/65%.

https://doi.org/10.1021/acs.jmedchem.0c02143
J. Med. Chem. 2021, 64, 4677−4696

Scheme 2. Preparation of Racemic 38a−e—Referring to Retrosynthetic Pathway C[a]

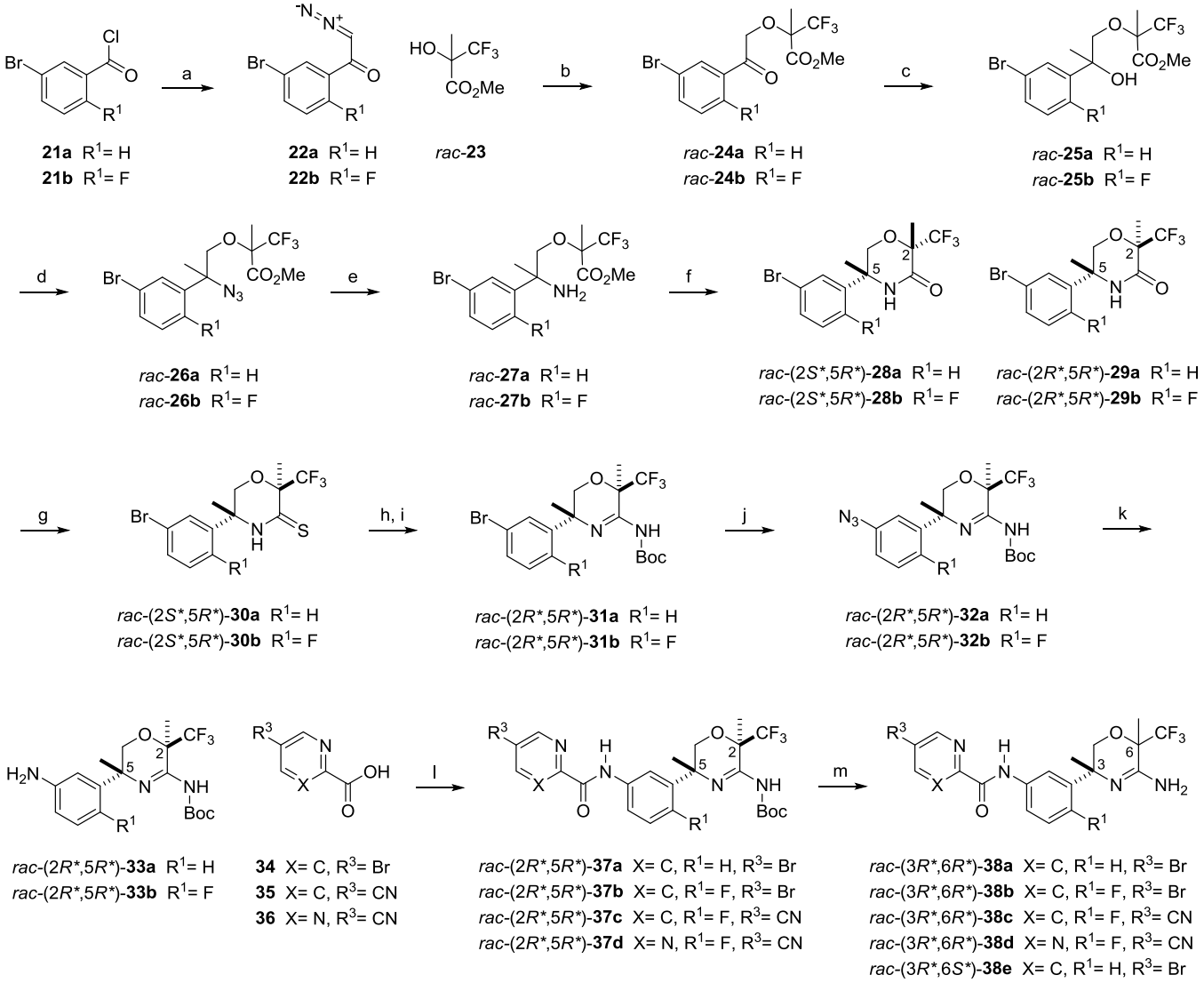

[a]Reagents and conditions: (a) $TMSCH_2N_2$, NEt_3, THF, 0.25 °C, 73/88%; (b) **23**, $Rh_2(TFA)_4$, CH_2Cl_2, 25 °C, 35/34%; (c) MeLi, $AlMe_3$, toluene, −78 °C, 69/65%; (d) $TMSN_3$, BF_3-Et_2O, toluene, 35 °C, 78/63%; (e) In, 4 N HCl-THF, 25 °C, 76/71%; (f) $AlMe_3$, CH_2Cl_2, 40 °C, (47/50%)/(38/44%); (g) P_2S_5, hexamethyldisiloxane, toluene, 100 °C, 95/85%; (h) *t*-BuOOH, NH_3, THF, 0−25 °C; (i) $(Boc)_2O$, NEt_3, acetonitrile, 25 °C, two steps 56%/57%; (j) NaN_3, CuI, (1*R*,2*R*)-*N*1,*N*2-dimethylcyclohexane-1,2-diamine, Na-ascorbate, EtOH-H_2O, 70 °C, 82%/-; (k) H_2, 10% Pd-C, EtOH, 25 °C, 61%/two steps 51%; (l) **34**, **35**, or **36**, EDC, HOAt, *N*,*N*-diisopropylethylamine, DMF, 25 °C; (m) 4 N HCl in dioxane, 40 °C, two steps 33−85%.

5-amino-1,4-oxazine headgroup in compound class **A** is not feasible, and alternative pathways had to be identified. The neopentylic 1,2-ether formation (Path B) was judged to be very difficult, and only an intramolecular bond forming process was given some consideration initially. We expected an intermolecular ether formation to **C** starting with the commercially available tertiary alcohol **D** and a sterically less demanding reactive electrophile (Path C) to be more promising. Subsequent asymmetric addition of a methyl group to a chiral sulfoximine intermediate derived from ketone **C** would install the chiral amine for lactam formation. Immediate addition of the C3 methyl group to the ketone and transformation of the tertiary alcohol into an amine with subsequent lactam formation would instead lead to the achiral 3,3,6,6-*tetra*-substituted 5-amino-1,4-oxazine headgroup, the common central intermediate of the different pathways. Alternatively, the attractive but somewhat more speculative 5-amino-1,4-oxazine formation by an intramolecular iodo-amidination reaction was considered as well (Path D), utilizing the amidine fragment (**E**), generated from **D** *via* allylic ether formation and subsequent transformation of the ester moiety into the corresponding amidine fragment.

After identification of the required absolute configuration at C6, the development of a more versatile synthetic route to the chiral key intermediate **G** was required to facilitate the P3 optimization process. The formation of the neopentylic ether linkage with an advanced chiral P1 fragment together with the chiral *tert*-alcohol **D** was initially considered attractive, but no precedence for such transformation was found in the literature at the time this work was started. Determined to find a more efficient synthesis, we hypothesized that an activated aziridine might be sufficiently reactive for a nucleophilic ring-opening with the *tert*-alkoxyde **D** (Path E). By this unprecedented key transformation, the common key amidine intermediate **G**

https://doi.org/10.1021/acs.jmedchem.0c02143
J. Med. Chem. 2021, 64, 4677−4696

Scheme 3. Preparation of 54—Referring to Retrosynthetic Pathway D[a]

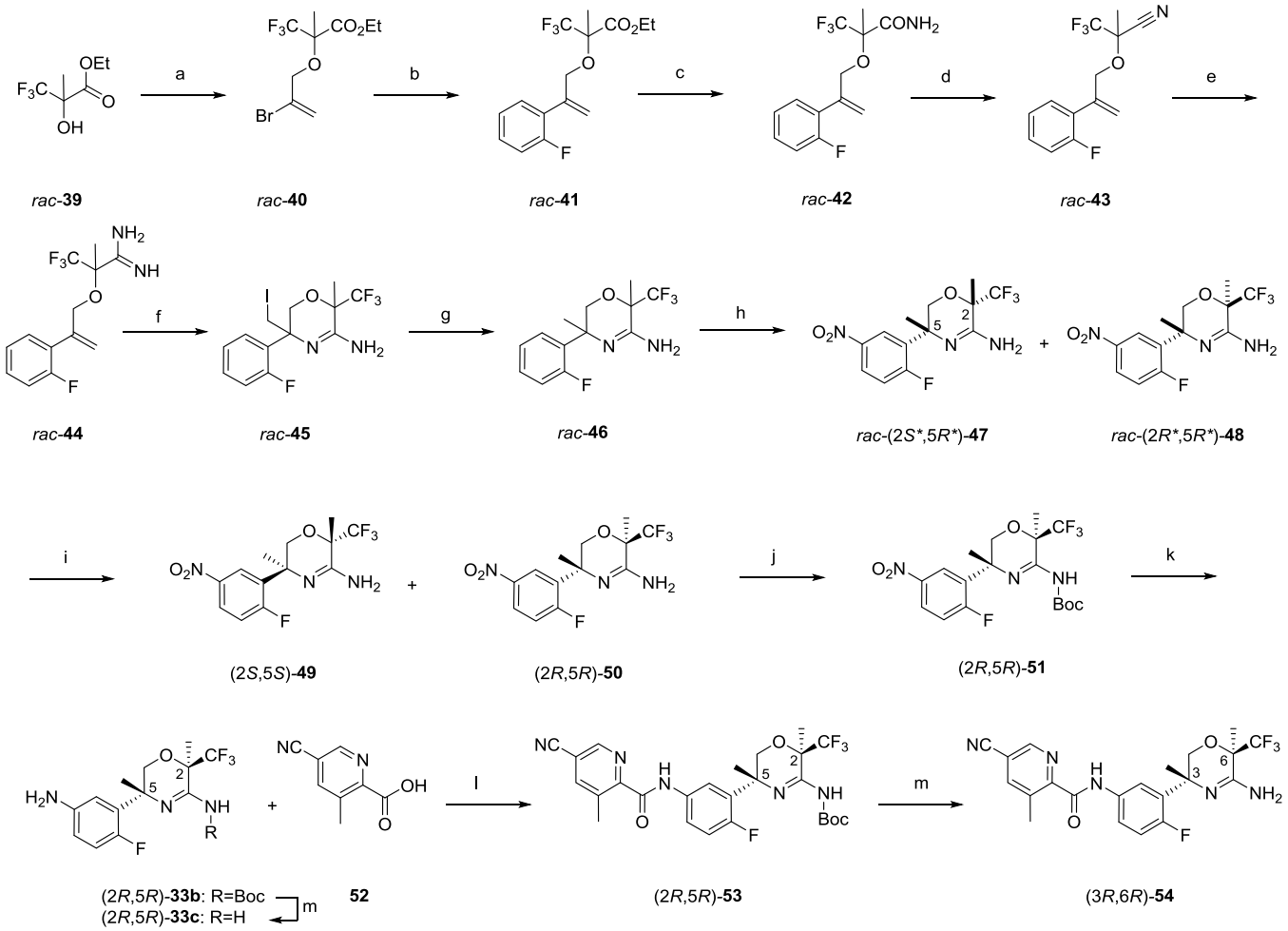

[a]Reagents and conditions: (a) NaH, 2,3-dibromoprop-1-ene, DMF, 25 °C, 81%; (b) (2-fluorophenyl)boronic acid, $Pd(PPh_3)_4$, CsF, DMF-H_2O 10:1, 65 °C, 64%; (c) 7 N NH_3 in MeOH, 55 °C, 98%; (d) trifluoroacetic anhydride, NEt_3, CH_2Cl_2, 5−25 °C, 93%; (e) 7 N NH_3 in MeOH, *N*-acetyl-L-cysteine, 80 °C, 96%; (f) I_2, Na_2CO_3, $CHCl_3$, 100 °C, 44%; (g) H_2, 10 Pd-C, NaOAc, MeOH, 25 °C, 97%; (h) KNO_3, H_2SO_4, 0 °C, 39/46%; (i) CHIRALPAK AD-H 5, CO_2-*i*-PrOH 90:10, 48/48%; (j) $(Boc)_2O$, NEt_3, acetonitrile, 25 °C, 90%; (k) H_2, 5% Pd-C, *i*-PrOH-THF 2:1, 50 °C, 92%; (l) EDC, HOAt, *N,N*-diisopropylethylamine, DMF, 25 °C, 81%; (m) CF_3COOH, CH_2Cl_2, 25 °C, 83%.

would become readily available *via* the corresponding amino-nitrile intermediate.

The synthesis of the C6-unsubstituted 5-amino-1,4-oxazine lead compounds **4** (R^1 = H) and *rac*-**20** (R^1 = F) is depicted in Scheme 1. The chloroacylated amino alcohols *rac*-**7a** and *rac*-**7b** were easily obtained from the corresponding commercially available amino acids *rac*-**5a** and *rac*-**5b** by borane reduction and acylation with chloroacetyl chloride. Cyclization to the 3,3-disubstituted morpholin-5-one *rac*-**8a** and *rac*-**8b** with *t*-BuOK followed by thioamide formation with Lawesson's reagent and oxidative-mediated transformation into the amidine with *tert*-butyl hydroperoxide/ammonia and subsequent *N*-Boc protection with Boc-anhydride provided the masked headgroup intermediates *rac*-**11a** and *rac*-**11b**. Transformation of the corresponding aryl-bromide into the anilide **13, 14**, and *rac*-**16** was carried out *via* Cu-catalyzed azide substitution and subsequent catalytic reduction with the Lindlar catalyst followed by a separation of the enantiomers **13** and **14** on the chiral stationary phase (Chiralpak IA). Finally, the target compound **4** and the C4-fluorinated analogue *rac*-**20** were obtained *via* 1-ethyl-3-(3-dimethylaminopropyl)carbodiimide (EDC)-mediated coupling with the P3 fragment **17** followed by *N*-Boc deprotection.

The synthesis of the highly substituted 5-amino-3,6-dimethyl-6-trifluoromethyl-1,4-oxazine containing inhibitors *rac*-(3*R**,6*R**)-**38a,e** (R^1 = H) and *rac*-(3*R**,6*R**)-**38b−d** (R^1 = F) following path C in Figure 3 is depicted in Scheme 2. Starting from the acid chlorides **21a** or **21b**, the diazoketones **22a** and **22b** were prepared with trimethylsilyldiazomethane. Subsequent Rh-catalyzed O−H insertion on the *tert*-alcohol *rac*-**23** provided the *tert*-ethers *rac*-**24a** and *rac*-**24b**. Chemoselective addition of the methyl group was achieved with trimethylaluminium at low temperature. The resulting racemic diastereomeric tertiary benzylic alcohol **25a** or **25b** was converted into azide **26a** or **26b** with trimethylsilyl-azide and boron trifluoride diethyl etherate in toluene at a slightly elevated temperature. Indium-mediated reduction of the azides under acidic conditions at ambient temperature provided the *tert*-amino-ester **27a** or **27b**, which upon treatment with trimethylaluminium delivered the lactams *rac*-(2*S**,5*R**)-**28a** and *rac*-(2*R**,5*R**)-**29a** or *rac*-(2*S**,5*R**)-**28b** and *rac*-(2*R**,5*R**)-**29b**, respectively. The diastereoisomeric pairs could be easily separated by flash chromatography, and the

https://doi.org/10.1021/acs.jmedchem.0c02143
J. Med. Chem. 2021, 64, 4677−4696

Scheme 4. Preparation of 54 and 64a−j—Referring to Retrosynthetic Pathway E[a]

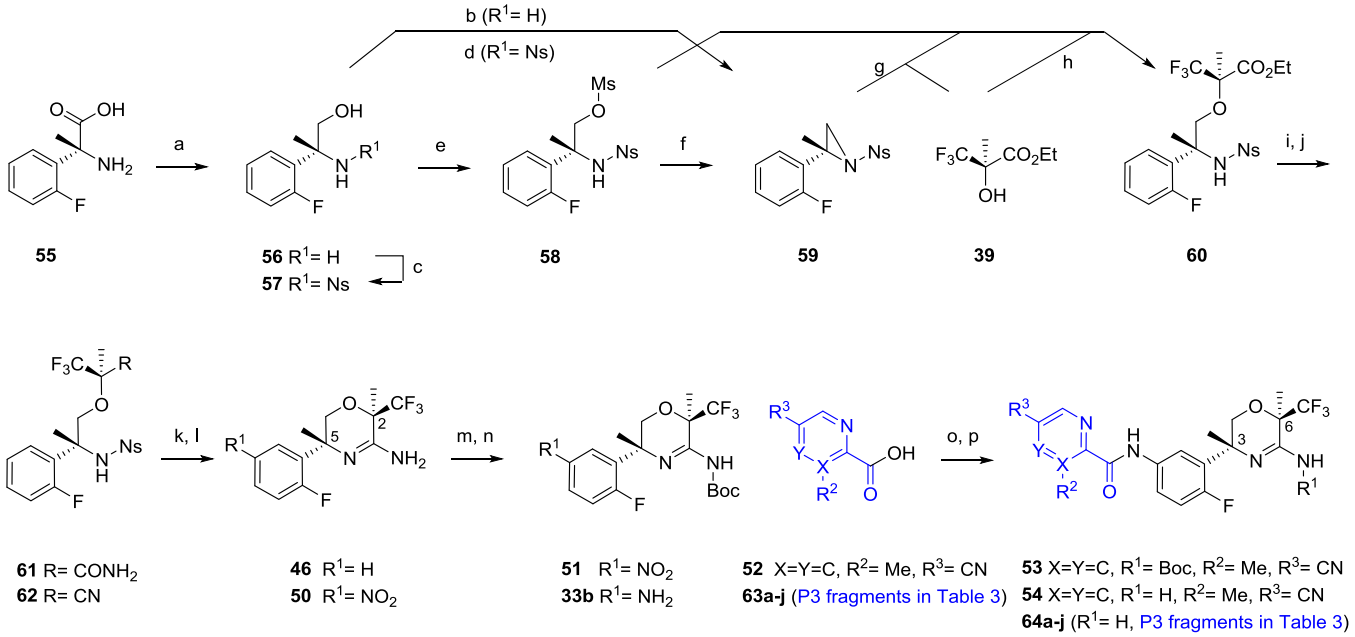

[a]Reagents and conditions: (a) BH_3 Me_2S, THF, 65 °C, 99%; (b) 4-nitrobenzene-1-sulfonyl chloride, $KHCO_3$, and Cs_2CO_3, acetonitrile, 80 °C, 50%; (c) 4-nitrobenzene-1-sulfonyl chloride, NMM, acetonitrile, 0−25 °C, 88%; (d) (i) mesyl chloride, 4-methylmorpholine, acetonitrile, 0−5 °C, (ii) NMM, acetonitrile, 30 °C, 84%; (e) mesyl chloride, NMM, acetonitrile, 0−5 °C, 95%; (f) DBU, CH_2Cl_2, 5−30 °C, 73%; (g) (*R*)-ethyl 3,3,3-trifluoro-2-hydroxy-2-methylpropanoate, *t*-BuOK, DMF/THF, 35 °C, 87%; (h) (*R*)-ethyl 3,3,3-trifluoro-2-hydroxy-2-methylpropanoate, 1 M *t*-BuOK in THF, DMF, 20−35 °C, 72%; (i) 7 N NH_3 in MeOH, 50 °C, 99%; (j) trifluoroacetic anhydride, NEt_3, CH_2Cl_2, 0−5 °C, 95%; (k) K_2CO_3, *N*-acetyl-L-cysteine, EtOH, 80 °C, 92%; (l) KNO_3, H_2SO_4, 0−5 °C, 81%; (m) $(Boc)_2O$, NEt_3, CH_2Cl_2, 0−25 °C, 90%; (n) H_2, 5% Pd-C, dioxane, 45 °C, 92%; (o) **63a−j**, EDC, HOAt, *N,N*-diisopropylethylamine (DIPEA), DMF, 5−25 °C, 16−92%; (p) CF_3COOH, CH_2Cl_2, 25 °C, 62−95%.

relative configuration of the individual diastereoisomers was assigned by NMR. In analogy to the sequence for C6-unsubstituted amino-oxazines (Scheme 1), the *N*-Boc protected amidines *rac*-(2*R**,5*R**)-**31a** and *rac*-(2*R**,5*R**)-**31b** were obtained *via* their thiolactams *rac*-(2*R**,5*R**)-**30a** and *rac*-(2*R**,5*R**)-**30b**, respectively, prepared with phosphorus pentasulfide and hexamethyldisiloxane in toluene.[56] Subsequent oxidative-mediated transformation into the amidine with *tert*-butyl hydroperoxide/ammonia followed by *N*-Boc protection completed the sequence. Cu-catalyzed substitution of the aryl-bromides by sodium azide followed by catalytic hydrogenation of *rac*-(2*R**,5*R**)-**32a** and *rac*-(2*R**,5*R**)-**32b** with palladium on carbon provided the anilines *rac*-(2*R**,5*R**)-**33a** and *rac*-(2*R**,5*R**)-**33b**, respectively. Amide formation with the P3 fragments **34, 35**, and **36** followed by acid-catalyzed *N*-Boc deprotection provided *rac*-(3*R**,6*R**)-**38a,e** and the fluorinated analogues *rac*-(3*R**,6*R**)-**38b−d**. Having determined the required relative configuration at C6 with the individual synthesis of *rac*-(3*R**,6*R**)-**38a** and *rac*-(3*R**,6*S**)-**38e**, a more viable synthesis of the 5-amino-6-methyl-6-trifluoromethyl-1,4-oxazine headgroup possessing the desired pK_a had to be identified.

Starting from an allylic ether bearing already the chiral C5−C6 amidine fragment, an intramolecular iodo-amidination reaction was explored to assemble the 3,3,6,6-*tetra*-substituted 5-amino-1,4-oxazine scaffold **G** (Path D, Figure 3). As shown in Scheme 3, the allylic ether *rac*-**41** was prepared initially from racemic ethyl 3,3,3-trifluoro-2-hydroxy-2-methylpropanoate (*rac*-**39**) and 2,3-dibromoprop-1-ene followed by a Suzuki coupling of *rac*-**40** with 2-fluorophenylboronic acid. Conversion of the ethyl ester *rac*-**41** to the amidine bearing allylic ether *rac*-**44** was achieved by aminolysis with NH_3 in methanol, conversion of the amide *rac*-**42** to the nitrile *rac*-**43** with TFAA-NEt_3, and final amidine formation with 7 N NH_3 and *N*-acetyl-L-cysteine in methanol at 80 °C.[57] All attempts to achieve an asymmetric intramolecular iodo-amidination with chiral oxazolidine and amino acid auxiliaries attached to the amidine moiety, as reported for the related iodo-lactamizations, failed.[58]

On the other hand, an achiral iodo-amidination with the unsubstituted amidine *rac*-**44** using iodine and Na_2CO_3 in chloroform at 100 °C led to the formation of a 1:1 mixture of racemic diastereoisomeric iodo-amidines *rac*-**45** in moderate yield.[59] Hydrogenolytic removal of iodine with 5% Pd-C in methanol containing NaOAc and subsequent nitration of *rac*-**46** with KNO_3 in H_2SO_4 followed by chromatographic separation of the *rac*-(2*S**,5*R**)-**47** and *rac*-(2*R**,5*R**)-**48** diastereoisomers and separation of the enantiomers of *rac*-(2*R**,5*R**)-**48** by SFC provided (2*S*,5*S*)-**49** and (2*R*,5*R*)-**50**. The remaining transformation to the aniline (2*R*,5*R*)-**33b**, the key intermediate for the further evaluation of P3 SAR, consisted of *N*-Boc-protection of the nitro-amidine derivative (2*R*,5*R*)-**50** and catalytic reduction of the aryl-nitro group of (2*R*,5*R*)-**51**. The final conversion of aniline (2*R*,5*R*)-**33b** into inhibitor (3*R*,6*R*)-**54** was initiated by EDC-mediated coupling with the P3 fragment **52** followed by acid-catalyzed *N*-Boc deprotection of (2*R*,5*R*)-**53** with TFA in dichloromethane. To enable the quantification of a potential metabolite, some **33b** was converted into aniline **33c**.

The most practical route to the key intermediate **33b** (Path E, Figure 3), exploiting the nucleophilic opening of a chiral aziridine with a chiral alkoxy C5−C6 fragment, is depicted in Scheme 4. The chiral amino alcohol **56**, prepared *via* borane reduction of **55**,[60] was initially transformed by a one-step

https://doi.org/10.1021/acs.jmedchem.0c02143
J. Med. Chem. 2021, 64, 4677−4696

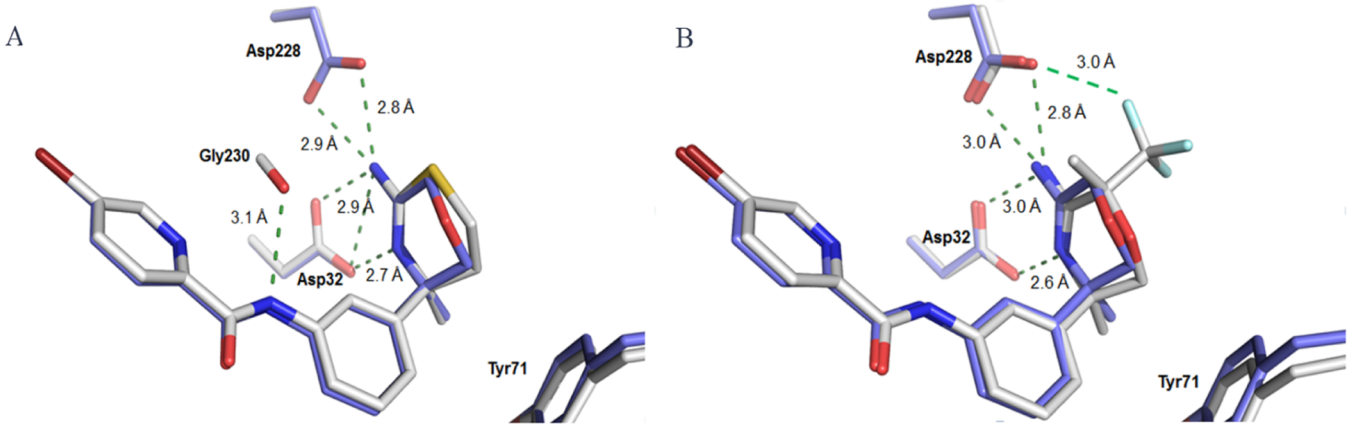

Figure 4. Superimposition of cocrystal structures of compounds bound to BACE1. (A) 5-Amino-1,4-oxazine inhibitor **4** (blue) with 2-amino-1,3-thiazine inhibitor **3** (white); PDB ID: 6FGY and 7B1E. (B) **4** (blue) with **38a** (white); PDB ID: 6FGY and 7B1P.

process with excess Ns-Cl and $KHCO_3$ in refluxing acetonitrile into the nosylated aziridine **59**. However, this procedure was not scalable and was replaced by a reproducible two- or three-step process requiring no chromatographic separation. Initial nosylation with Ns-Cl/NMM at 0−5 °C in acetonitrile provided selectively the *N*-nosylated amino alcohol **57**, which upon *O*-mesylation with Ms-Cl/NMM in acetonitrile at 0−5 °C delivered crystalline **58** in excellent yield. Addition of excess base and increasing the temperature to 30 °C led directly to the formation of nosylated aziridine **59**. Alternatively, **59** can be generated from **58** with 1,8-diazabicycloundec-7-ene (DBU) in dichloromethane at ambient temperature. The opening of aziridine **59** with the chiral *tert*-alcohol **39** worked best with *t*-BuOK as the base in anhydrous *N,N*-dimethylformamide at 35 °C. By a controlled acidic workup, the highly functionalized ether intermediate **60** can be obtained in the crystalline form. Alternatively, the ether intermediate **60** can be obtained directly from the crystalline mesylate **58** and chiral *tert*-alcohol **39** with excess *t*-BuOK in *N,N*-dimethylformamide. Conversion of the ethyl ester **60** to the nitrile bearing ether **62** was achieved by aminolysis with NH_3 in methanol and conversion of amide **61** to nitrile **62** with TFAA-NEt_3. Removal of the nosyl protecting group and subsequent formation of the 3,3,6,6-*tetra*-substituted 3-amino-1,4-oxazine **46** were achieved in one step with K_2CO_3 and *N*-acetyl-L-cysteine in ethanol at 80 °C. The transformation of **46** into the key intermediate **33b** followed the same 3-step reaction sequence as previously described for the preparation of anilide **33b** in Scheme 3. The final conversion of **33b** into **64a−j**, bearing the different P3 fragments **63a−j**, followed the same 2-step reaction sequence previously described for (3*R*,6*R*)-**54** in Scheme 3.

RESULTS AND DISCUSSION

The X-ray co-crystal structure of the initial 6-unsubstituted 5-amino-1,4-oxazine derivative **4** with BACE1 (Figure 4A) confirmed an optimal binding arrangement of the amidine with the catalytic aspartates Asp32 and Asp228 (2.7−2.9 Å).[51] In addition, we learnt that the NH of the amide of **4** formed an about equally strong hydrogen bond with the backbone carbonyl of Gly230 as the 2-amino-thiazine inhibitor **3** (3.0 Å for **3** vs 3.1 Å for **4**), in agreement with the nearly equal potency when the same P1−P3 fragment is used (IC_{50} 44 nM for **3** vs 70 nM for **4**). Closer examination of the binding mode of the prototype compound **4** confirmed that a small electron-withdrawing substituent like a CF_3 group at C6, to reduce the pK_a from 9.5 to ∼7,[52] could be tolerated. Since disubstitution at C6 was considered to be essential to ascertain sufficient configurational, chemical, and metabolic stability, the absolute stereochemistry at C6 could not entirely be predicted by modeling. Therefore, the diastereoisomeric pair *rac*-(3*R**,6*R**)-**38a** and *rac*-(3*R**,6*S**)-**38e** was synthesized. The inhibitor *rac*-(3*R**,6*R**)-**38a** was found to be 50-fold more potent over *rac*-(3*R**,6*S**)-**38e**. Subsequently, the optimal binding of the (6*R*)-configuration was confirmed in the co-crystal structure with BACE1 (Figure 4B). In addition, the insertion of fluorine at C4 of the P1 phenyl ring was considered to be beneficial to reduce the formation of a possibly toxic aniline metabolite (**33c**) by hydrolysis of the P3−amide bond *in vivo*. As expected, this remote modification had only a minor effect on the pK_a of the amidine (pK_a 9.5 for **4** vs 9.3 for *rac*-**20**, respectively, and 7.3 for *rac*-(3*R**,6*R**)-**38a** vs 7.0 for *rac*-(3*R**,6*R**)-**38b**) but led to a ∼2-fold increased *in vitro* potency (IC_{50} 20 nM for *rac*-(3*R**,6*R**)-**38a** vs 11 nM for *rac*-(3*R**,6*R**)-**38b**, Table 2). The improvement in inhibitory potency may be driven by electrostatic interactions of the fluorine with Tyr71 and Phe108, which are in close proximity (3.0 Å), as observed in the co-crystal structure of **38a** in Figure 4. Similar potentially beneficial electrostatic interactions of the fluorine atoms of the CF_3 group with the carbonyl of Asp228 (3.0 Å) and the surrounding water network interacting with Thr72 of the flap can be envisaged, besides shielding of the H-bonding network between the polar amidine headgroup and the two catalytic aspartates Asp228 and Asp32, providing a 5-fold increase in potency (IC_{50} 58 nM for *rac*-**20** vs 11 nM for *rac*-(3*R**,6*R**)-**38b**). The identification of this highly potent 6-methyl-6-trifluoromethyl-substituted 5-amino-1,4-oxazine headgroup with an optimal pK_a of 7.0, still allowing protonation in the acidic environment in which BACE1 is active, however, was set off by its rather demanding synthetic accessibility. Excellent BACE1 inhibition in its native cellular environment could be demonstrated with inhibitor *rac*-(3*R**,6*R**)-**38b** in wtAPP CHO cells (IC_{50} 22 nM), as well as a very high selectivity against human cathepsin D (IC_{50} > 250 μM), for this BACE inhibitor with an amide linker between P1 and P3 substituents, compared to shorter biaryl P1−P3 extensions.[61] Equally important, a good permeation (P_{app} = 67 nm/s) and a very low P-gp-mediated efflux (ER = 1.4) in MDCK cells transfected with human MDR1 could be observed, which could be pointing to good brain penetration.

https://doi.org/10.1021/acs.jmedchem.0c02143
J. Med. Chem. 2021, 64, 4677−4696

Table 2. *In Vitro* Profile of the Initial 5-Amino-1,4-oxazine Lead Compounds[51f]

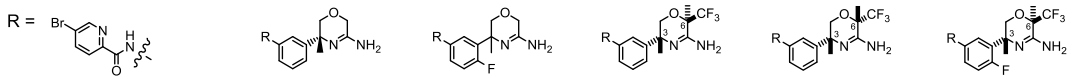

	4	*rac*-**20**[a]	*rac*-(3*R**,6*R**)-**38a**[a]	*rac*-(3*R**,6*S**)-**38e**[a]	*rac*-(3*R**,6*R**)-**38b**[a]
hBACE1 IC_{50} [μM][b]	0.070	0.058	0.020	1.08	0.011
wtAPP-CHO IC_{50} [μM][b]	0.017	0.003	0.032	1.16	0.022
hCathD IC_{50} [μM][b]	>10	>10	73	139	>250
calculated pK_a[c]	6.2	6.0	4.8	4.8	4.5
measured pK_a[d]	9.5	9.3	7.3	7.3	7.0
MDCK P_{app} [nm/s][e]	190	124	103	49	67
ER[f]	30	8.2	1.9	1.6	1.4

[a]Racemic compounds. [b]Values are means of at least three experiments. [c]Calculated using Advanced Chemistry Development (ACD/Labs) Software V9.06 (1994-2005 ACD/Labs). [d]Measured pK_a determined by potentiometric titration.[62] [e]P_{app} is the permeability through an MDR1−MDCK cell monolayer. [f]ER is the efflux ratio (P_{BL-AP}/ P_{AP-BL}) in MDCK cells transfected with human MDR1.

Table 3. P3 Structure−Activity Relation

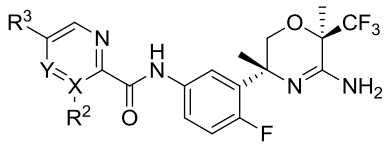

cmpd	R^2	R^3	X	Y	BACE1 IC_{50} [μM][b]	BACE2 IC_{50} [μM][b]	CathD IC_{50} [μM][b]	wtAPP CHO IC_{50} [μM][b]	ER[c]	CYP450 3A4/2D6/2C9 IC_{50} [μM]	brain Aβ40 red.[d] [%]	metabolite **33c**[d] [% of parent]
38b[a]	H	Br	C	C	0.011	0.003	>250	0.022	1.4	17/0.9/3		
64a		Br	N	C	0.016	0.003	180	0.005	3.4	8/>20/>20		
64b[a]		CN	N	C	0.034	0.004	>250	0.024	17	>20/>20/>20		
64c	H	CN	C	C	0.006	0.007	>250	0.009	2	>20/>20/>20	75	14.3
54	Me	CN	C	C	0.005	0.005	>250	0.003	1.9	>20/>20/>20	79	0.16
64d	Me	CN	C	N	0.062	0.130	>250	0.105	3.5	>20/>20/>20		
64e	Cl	CN	C	C	0.006	0.005	>250	0.004	3.7	17/>20/>20	71	<0.2[e]
64f	NH_2	CN	C	C	0.005	0.005	30	0.004	2.0	7/12/>20		
64g	Me	OMe	C	C	0.033	0.004	>250	0.017	nd	>20/9/>20		
64h	Me	$OCHF_2$	C	C	0.014	0.012	>250	0.006	1.2	20/4/>20		
64i	Cl	$OCHF_2$	C	C	0.016	0.017	>250	0.009	1.9	4/7/17	56	<0.2[e]
64j	Cl	Cl	C	C	0.008	0.002	>250	0.022	1.6	>20/11/>20	66	0.3

[a]Racemic compounds. [b]Values are means of at least three experiments. [c]ER is the efflux ratio (P_{BL-AP}/P_{AP-BL}) in MDCK cells transfected with human MDR1. [d]Percent brain Aβ reduction in rats (n = 5) 4 h post dosing of 10 μmol/kg p.o. relative to vehicle-treated animals. [e]Below LLOQ of LC-MS quantification.

During the course of our work, we as well as other groups[39,49] explored a wide variety of oxazine-derived scaffolds to identify BACE1 inhibitor headgroups with a promising *in vitro* activity and physicochemical profile and better synthetic accessibility. However, in view of the difficulties in achieving a superior physicochemical profile, the 5-amino-6-methyl-6-trifluoromethyl-1,4-oxazine headgroup merited extra effort to identify a scalable synthesis. In parallel, the identification of the most efficacious and druglike P3 substituent was performed.

Early SAR exploration and the co-crystal structures of **4** and *rac*-**38a** (Figure 4) suggested that the important amide NH hydrogen bond to the backbone carbonyl of Gly230 is impeded by an sp^2 C−H group *ortho* to the carbonyl of the amide linking the P3 to the P1 fragment. We therefore focused our P3 exploration on various 2-substituted pyridine, pyrazine, and pyrimidine fragments (Table 3). At the beginning of our SAR exploration, the 5-bromopicoline fragment was used to compare the physicochemical and activity profiles of the different headgroups. However, this P3 fragment was not suitable for *in vivo* profiling due to the high *in vitro* clearance in rat liver microsomes (CL_{int} 154 μL/min·mg for *rac*-**38a** and 62 μL/min mg for *rac*-**38b**) and inhibition of CYP450 isoforms 2D6 (IC_{50} 0.9 μM for *rac*-**38b**) and 2C9 (IC_{50} 3 μM for *rac*-**38b**). Only a partial improvement of the metabolic profile was observed by substituting the pyridine with the less lipophilic pyrimidine as shown in **64a**, preserving the potency but increasing the ER to 3.4. Substitution of the bromine with a cyano group in *rac*-**64b** produced a clean CYP450 enzyme inhibition profile, however at the expense of a large increase in the ER (3.4 to 17). The combination of the cyano group in *rac*-**64b** with the less efflux-prone pyridine fragment decreased the ER from 17 to 2. In addition, the high selectivity against human Cathepsin D (>40 000-fold) was retained and the cellular potency of **64c** was comparable (IC_{50} 9 nM for **64c** vs 24 nM for *rac*-**64b**). Furthermore, a clean CYP450 profile was obtained (all IC_{50} > 20 μM), making **64c** the first valid candidate for a PK/PD experiment in rats. The introduction of a methyl group at C3 adjacent to the carbonyl moiety in the pyridine ring, to impede amide hydrolysis *in vivo*, was well-tolerated and gratifyingly led to a further improvement of the cellular potency (IC_{50} 3 nM for **54** vs 9 nM for **64c**), preserving the clean CYP450 profile. In an attempt to further

https://doi.org/10.1021/acs.jmedchem.0c02143
J. Med. Chem. 2021, 64, 4677−4696

lower the lipophilicity, the pyrazine compound **64d** was prepared. Only a moderate increase in the ER was observed compared to the pyrimidine (3.5 for **64d** vs 17 for *rac*-**64b**), however, at the expense of a >5-fold lower cellular potency (IC_{50} 24 nM for *rac*-**64b** vs 105 nM for **64d**). Interestingly, **64d** showed as an only example a slight preference (2-fold) for inhibition of BACE1 over BACE2, while for all other examples, no or even 8-fold preference for inhibition of BACE2 (**64b,g**) was observed. Substitution of the methyl group at C3 of the pyridine by Cl (**64e**) and NH_2 (**64f**) produced the equipotent analogues **64e** and **64f**, however, with a less clean metabolic CYP450 profile. Replacement of the cyano group on the pyridine fragment with OMe (**64g**) and $OCHF_2$ (**64h,i**) delivered analogues of slightly lower potency and inferior metabolic profiles, especially for **64i**. Substitution of the cyano and the Me group with Cl produced a nearly equipotent analogue (IC_{50} 8 nM for **64j** vs 6 nM for **54**), however, with lower cellular potency (IC_{50} 3 nM for **54** vs 22 nM for **64j**) and only moderate metabolic stability for the rather lipophilic derivative ($\Delta C \log P$ of 1) compared to the best inhibitor **54** in Table 3.

Only compounds with a promising cellular potency (IC_{50} < 10 nM), minimal *in vitro* P-gp efflux (ER < 5), and no metabolic liabilities were selected for *in vivo* PK/PD evaluation. Brain Aβ40-lowering was determined after oral administration in rats (Sprague-Dawley, $n = 5$) 4 h post dosing. Blood and brain samples were taken to assess compound levels as well as the percentage of Aβ reduction in the forebrain and optionally also in CSF. Concerned about the potential formation of the undesired aniline metabolite **33c** by metabolic cleavage of the amide moiety, the amounts of **33c** in blood were routinely coquantified with the parent compound. Indeed, considerable amounts of this metabolite were observed with our first PK/PD candidate **64c** (14.3%, Table 3). With the insertion of a small substituent at C3 adjacent to the P3-P1 linking carboxamide of **64c**, for example, a methyl, chlorine, or NH_2 group (R^2 in Table 3), formation of the aniline metabolite was almost eliminated, as shown in Table 3 by comparison of compound **64c** with **54**, **64e**, **64i**, and **64j**. The most robust brain Aβ-lowering effect after 4 h was observed with **54** (−79%), **64e** (−71%), and **64j** (−66%) after application of an oral dose of 10 μmol/kg in rats (Table 3). Compound **54** possessed the most favorable *in vitro* properties (cellular IC_{50} 3 nM, >50 000-fold selectivity over human Cathepsin D, inhibition constants for CYPs 3A4, 2D6, and 2C9 above 20 μM, and a low P-gp efflux ratio of 1.9). An extended overall profile of **54** is shown in Table 4, and the binding to BACE1 is shown in Figure 5.

From the candidates selected for an *in vivo* efficacy experiment, compound **54** revealed also the best overall PK parameters (highest area under the curve (AUC) of 973, C_{max} of 128, medium CL, and low V_{ss}), as shown in Table 5. PK studies of **54** in mice and dogs showed a lower clearance and volume of distribution in mice than in rats (mice vs rats: CL 16 vs 26, V_{ss} 4.6 vs 9.0) and even much lower values in dogs (dogs vs rats: CL 0.4 vs 26, V_{ss} 0.9 vs 9.0).

Having achieved moderate-to-high oral bioavailability in mice, rats, and dogs (37, 77, and 62%, respectively), compound **54** (**NB-360**) was further evaluated in animal models including those displaying characteristics of amyloid pathology.[63] In summary, NB-360 reduced Aβ40 by >80% in the rat brain and CSF 8 h after oral doses (0.3−30 μmol/kg). The **NB-360** unbound fraction (AUC) was 0.63 μM·h in rat blood and 0.54 μM·h in rat brain, showing an almost equal distribution of the compound in both tissues and the absence of significant efflux at the blood−brain barrier. A single 0.5 mg/kg oral dose of **NB-360** in dogs carrying a ventricular port for repeated CSF collection reduced Aβ peptide 1−40 by more than 80% and remained significantly inhibited for at least 72 h.[63]

Chronic treatment of APP-transgenic mice with 100 μmol/kg **NB-360** q.d. for 6 weeks led to a significant reduction of APP fragments C99, sAPPβ, Aβ 1−38, 1−40, and 1−42. Amyloid plaques were profoundly reduced compared to vehicle-treated animals, staying at baseline levels. Furthermore, treatment with **NB-360** strongly reduced the number of activated microglia cells and astrocytes, markers of neuroinflammation.[63]

In mice chronically treated with **NB-360**, we observed the appearance of gray patches in the otherwise black fur. Others and we investigated this further, with data showing that inhibition of BACE2 is causally involved in hair depigmentation, probably *via* inhibition of the correct processing of the melanosome protein PMEL-17 and improper melanin distribution in the hair follicle.[64,65]

Table 4. Extended Profile of 54 (NB-360)

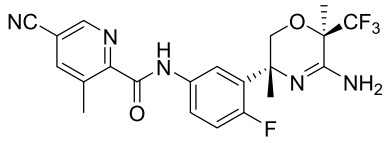

hBACE1 IC_{50} μM	0.005
hBACE2 IC_{50} μM	0.005
pepsin, hCathD, hCathE IC_{50} μM	>250
hAβ_{40} wtAPP CHO cell IC_{50} μM	0.003
hAβ_{40} SweAPP CHO cell IC_{50} μM	0.033
hAβ_{42} wtAPP CHO cell IC_{50} μM	0.003
sAPPβ wtAPP CHO cell IC_{50} μM	0.004
log P (octanol/water)	3.7
pK_a	7.1
log PAMPA (log Pe pH 6.8) [cm/s]	-3.6
MDR1−MDCK apical-basolateral (A−B) [nm/s]	141
MDR1−MDCK basolateral-apical (B−A) [nm/s]	263
MDR1−MDCK efflux ratio (B−A/A−B)	1.9
CYP P450 (3A4, 2D6, 2D9) IC_{50} μM	>20
hERG manual patch clamp IC_{50} μM	>30

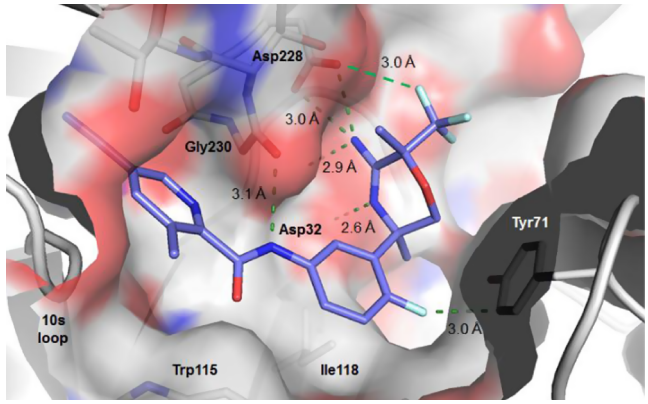

Figure 5. Co-crystal structure of **54** bound to human BACE1 (PDB ID: 7B1Q).

https://doi.org/10.1021/acs.jmedchem.0c02143
J. Med. Chem. 2021, 64, 4677−4696

Table 5. Pharmacokinetic Parameters in Rats, Mice, and Dogs

cmpd	species	dose [μmol/kg][a]	$AUC_{(0-\infty)}$ [nM·h][a,b]	C_{max} [nM][a,b]	%F	Hep. CL_{int} [μL/min/10^6 cells]	*in vivo* clearance [mL/min/kg][c]	V_{ss} [L/kg][c]	$t_{1/2}$ [h][c]
64e	rat	6[d]	511	74	61	98	43	8.6	2.8
64i	rat	6[d]	873	80	61	97	24	7.6	5.6
64j	rat	6[d]	564	83	70	74	47	7.1	2.3
54	rat	6[d]	973	128	77	17	26	9.0	4.9
54	mouse	6	882	152	37	n.d.	16	4.6	3.6
54	dog	0.67	67 370	1880	62	n.d.	0.4	0.9	36

[a]Oral (6 μmol/kg for rats and mice, 0.3 mg/kg for dogs). [b]Dose normalized. [c]Intravenous (2 μmol/kg for rats and mice, 0.1 mg/kg for dogs). [d]Cassette of five compounds with 6 μmol/kg.

The risk of unknown physiological consequences due to inhibition of BACE2 led to a discontinuation of development efforts for **NB-360**, but the excellent PK/PD properties of this compound have facilitated research efforts in mechanistic animal models related to BACE1 inhibition in the context of AD. For example, a combined histology/magnetic resonance imaging study in old APP-transgenic mice with vascular amyloid pathology addressed the question of the possible occurrence of microhemorrhages as a potential consequence of treatment with BACE1 inhibitors.[66] Antiamyloid-β antibody treatment in AD patients frequently resulted in cerebral microbleeds. We did not observe such bleedings in APP23 mice treated with **NB-360**, indicating that microhemorrhages are a consequence of the specific mechanism of action of antibodies, but not a direct consequence of blocking the generation of amyloid-β peptides *via* direct inhibition of BACE1. Furthermore, chronic studies performed with **NB-360** in APP-transgenic mice showed that BACE1 inhibition markedly reduces the increase of downstream neurodegeneration markers Tau protein and the neurofilament light chain, as well as deposition of vascular amyloid-β.[67−69]

CONCLUSIONS

In summary, we have reported the discovery of a novel 3-aryl substituted (3*R*,6*R*)-5-amino-3,6-dimethyl-6-trifluoromethyl-3,6-dihydro-2*H*-1,4-oxazine headgroup. Selective structural modifications at C6 of the 1,4-oxazine-based prototype compound **4** aimed at fine-tuning the pK_a and at shielding the amidine and ether oxygen as much as possible from undesired chemical and metabolic transformations. This resulted in the identification of a 3-aryl substituted (3*R*,6*R*)-5-amino-3,6-dimethyl-6-trifluoromethyl-3,6-dihydro-2*H*-1,4-oxazine headgroup bearing an optimal pK_a of ∼7.0. While retaining the good brain penetration properties of the initial lead compound **38a**, the potency, pharmacokinetics, and metabolic profile were further optimized by structure-based modifications of the P3 fragment. From the candidates with the best *in vitro* profile (cellular potency, minimal CYP and hERG liabilities, and low P-gp efflux ratio) and the most robust brain Aβ peptide reduction in rats (Table 3), compound **54** (**NB-360**) demonstrated an excellent overall profile (Table 4) and was selected for a more comprehensive PK/PD assessment in rats, dogs, and APP-transgenic mice. The lowering of pK_a of 1,4-oxazine with CF_3 substitution had a profound effect on activity and P-gp efflux. Further optimization of P3 improved metabolic stability, delivering with **NB-360** an orally active BACE1 inhibitor with an excellent PD profile in mice, rats, and dogs. Compound **NB-360** did not enter clinical trials in Alzheimer's disease since hair discoloration observed in mice was considered a sign for off-target inhibition of BACE2 occurring at therapeutic doses. Involvement of BACE2 in pancreatic β-cell function and melanoma cell proliferation is documented, and BACE2 may have other, yet undetected physiological functions.[70,71] This was considered a safety risk, in particular for long-term prevention trials. Another oxazine derivative, CNP520 (umibecestat), with a superior safety profile was identified and entered long-term trials in AD.[72] However, we decided to make **NB-360** available to a large number of interested academic institutions for preclinical studies. Using a potent tool compound in a standardized way, in terms of source, doses, and formulations, contributed significantly to deepening our understanding of the physiological function of BACE1. Furthermore, **NB-360** treatment of APP-transgenic mice led to the discovery of various aspects of BACE1 inhibition on Alzheimer's disease biomarkers, neuronal activity and networks, and to the kinetics of amyloid plaque growth.[73,74]

EXPERIMENTAL SECTION

***In Vitro* Potency and Profiling Assays.** Assays for human and mouse BACE1, human BACE2, porcine pepsin, and human cathepsin D and E were performed as described.[63] Cellular potency was determined in Chinese hamster ovary cells stably transfected with human APP751 as described.[63]

The octanol/water distribution coefficient was derived from the apparent permeability across an artificial liquid membrane.[75] The PAMPA assay was performed as described.[24] MDCK cells overexpressing human p-glycoprotein (MDR1−MDCK cells, obtained from Prof. A. Berns, Netherlands Cancer Institute) were grown on multiwell plates, 1 μm pore size (Becton Dickinson). After formation of a tight monolayer, test compounds were applied to either the upper or the lower chamber. After 1 h, liquid was removed from the upper and lower chambers and analyzed by high-performance liquid chromatography-mass spectrometry (HPLC-MS). Apical-to-basolateral and basolateral-to-apical transport rates were calculated.

Human CYP450 Enzymes Inhibition Assays. The following substrates were used to assess the reversible inhibition of the CYP450 enzymes: CYP3A4, midazolam; CYP2D6, Bufuralol; and CYP2C9, Diclofenac. Assays were performed in human liver microsomes supplemented with NADPH. Test compounds were diluted to 0.5−20 μM final concentrations. The incubation time was 10 min in 50 mM sodium phosphate buffer (pH 7.5). After stopping and centrifugation, analysis was performed using a solid-phase-extraction (SPE) mass spectrometry system consisting of a TSQ Quantum Discovery MAX mass spectrometer controlled by Xcalibur 3.0 and equipped with an electrospray ion source (Ion Max electrospray interface) from Thermo Fisher Scientific (Reinach, Switzerland) and a RapidFire high-throughput SPE system from Agilent Technologies (Waldbronn, Germany).

Animal Experiments. All animals were maintained under standard housing conditions with access to standard pelleted food and water ad libitum, throughout the experiments. Animal experiments were conducted in accordance with Swiss national animal welfare regulations, under the ethically approved animal experimenta-

https://doi.org/10.1021/acs.jmedchem.0c02143
J. Med. Chem. 2021, 64, 4677−4696

tion licenses authorized by the Cantonal Veterinary Authority of Basel City and the Federal Veterinary Office of Switzerland.

Pharmacokinetic studies used male Sprague-Dawley rats, C57BL6 mice, and Beagle dogs, obtained from Charles River (France, rodents) and Marshall (Italy, dogs). Compounds were dosed intravenously as a solution (NMP/PEG200-based mixtures), whereas for oral dosing, compounds were suspended in methylcellulose 0.5% (w/v)/99.5% water/0.1% Tween 80 and applied *via* oral gavage. Mouse blood was collected by sublingual bleeding or at sacrifice, whereas a serial blood sampling allowed obtaining individual PK profiles in rats and dogs. Blood samples were taken between 5 min (intravenous) and 15 min (oral) intervals and then longer, subsequently up to 24 h (mice), 48 h (rat), and 408 h (dog). Brain exposures were determined in the pharmacological studies by collecting the brain after decapitation at selected time points after dosing.

For bioanalytics, brain samples were homogenized with 2 mM KH_2PO_4 buffer (approx. 1/2, w/v). A structurally similar internal standard was added to the blood or brain homogenate samples, and compounds were extracted by quenching with a fourfold volume of acetonitrile and an aliquot of the supernatant was directly injected into the LC/MS/MS system. Separation from endogenous components was achieved using a reverse-phase column and a gradient elution with water/1% formic acid and acetonitrile/1% formic acid. BACE1 inhibitors were ionized with the positive electrospray mode and quantified in the MRM mode.

For rat pharmacokinetic/pharmacodynamics studies, male Charles River Sprague-Dawley rats of approx. 300 g body weight were used, and experiments were done as described before.[63]

X-ray Analysis. The catalytic domain of human BACE1 was expressed in *Escherichia coli* and refolded, as already described in Hanessian et al. (2015), Supporting Information.[76] The crystal structures of the complexes with **3**, **38a**, and **54** were obtained by soaking orthorhombic crystals of unliganded BACE1, grown at 19 °C from 15% PEG 1500 in water by the method of vapor diffusion in hanging drop using 15.0−16.4 mg/mL BACE1 (residues 46−447 of Uniprot entry P56817) in 10 mM Tris-HCl pH 7.4, 25 mM NaCl. The soaking buffer was 28.5−30.0% PEG 1500, 50 mM sodium citrate pH 5.2−5.5, with 1.0 mM compound and 0.9−1.8% DMSO. Crystals were directly flash-frozen, and diffraction data were collected either at the Swiss Light Source (SLS, in Villigen, Switzerland) beamline X10SA, with a MAR CCD 225 (compound **3**) or a Pilatus (compound **54**) detector, or in the laboratory (compound **38a**), using an FR-E superbright rotating anode X-ray generator and a SATURN92 CCD detector. All diffraction data were processed with XDS[77] as implemented in APRV.[78] The diffraction data extended to between 1.62 and 1.94 Å. All structures were determined by difference Fourier and refined using CNX[79] and Coot,[80] to crystallographic *R*-factors ranging from 18.6 to 18.9% (free *R*-factors ranging between 21.1 and 21.8%).

Synthesis. Unless otherwise mentioned, all reagents were obtained from commercial suppliers and used without further purification unless noted otherwise. Anhydrous solvents were obtained from Aldrich and used directly. All reactions involving air- or moisture-sensitive reagents were performed under a nitrogen or argon atmosphere. All microwave-assisted reactions were conducted with a Smith synthesizer from Personal Chemistry, Uppsala, Sweden. Silica gel chromatography was performed using either glass columns packed with silica gel (230−400 mesh) or prepacked silica gel cartridges from Isco. All NMR spectra were collected on a Bruker 360, 400, or 600 MHz or on a Varian 300 or 400 MHz spectrometer. The chemical shifts were expressed as ppm (δ units) with tetramethylsilane or residual protonated solvent used as the reference. All tested compounds were purified to ≥95% purity as determined by reverse-phase ultrahigh-pressure liquid chromatography (UPLC). UPLC analysis was obtained on a Waters ACQUITY UPLC and UPLC-MS. UPLC method A (2.0 min UPLC run): Acquity UPLC HSS T3 C18 column, 50 mm × 2.1 mm, 1.7 μm, 35 °C; mobile phase, *A* = 0.1% TFA in H_2O, *B* = 0.1% TFA in AcCN; gradient, 0.0−1.5 min, 5−100% B; flow rate 1 mL/min; 218 and 254 nM; 1 min post time; 1 μL injection. UPLC-MS (2.0 min UPLC run): Acquity UPLC HSS T3 C18 column, 50 mm × 2.1 mm, 1.8 μm, 50 °C; mobile phase, *A* = 0.05% formic acid + 3.75 mM ammonium acetate in H_2O, *B* = 0.04% formic acid in AcCN; gradient, 0.0−1.4 min, 2−100% B; flow rate 1.2 mL/min; 218 and 254 nM; 1 min post time; 1−5 μL injection. All assay compounds had a measured purity of ≥95% (by thin-layer chromatography (TLC) and UV) as determined using this analytical UPLC or UPLC-MS system. Low-resolution mass spectral (MS) data were determined on an Agilent 1100 mass spectrometer using ES ionization modes (positive and/or negative) and water-MeOH 3:7 + 2 of 25% ammonium hydroxide solution. High-resolution mass spectral (HRMS) analyses were performed using electrospray ionization in the positive ion mode after separation by liquid chromatography (Nexera from Shimadzu). The elemental composition was derived from the mass spectra acquired at the high resolution of about 30 000 on an LTQ Orbitrap XL mass spectrometer (Thermo Scientific). The high mass accuracy below 1 ppm was obtained using a lock mass.

The procedures for the syntheses of compounds **4** and *rac*-**20** (Scheme 1, retrosynthetic pathway A), compounds *rac*-(3*R**,6*R**)-**38a−d** and *rac*-(3*R**,6*S**)-**38e** (Scheme 2, retrosynthetic pathway C), and compound **54** (Scheme 3, retrosynthetic pathway D) are available in the supplementary part including the separation of (*rac*-**49**) and **50**. The final steps to **51**, **33b**, **53**, and **54** are identical, as described in procedure E.

Procedure for the Synthesis of Compounds 54 and 64a−64j (Scheme 4, Retrosynthetic Pathway E).

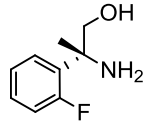

*(R)-2-Amino-2-(2-fluorophenyl)propan-1-ol Hydrochloride (**56**).* To a suspension of (*R*)-2-amino-2-(2-fluorophenyl)-propanoic acid hydrochloride (**55**) (34.0 g, 150 mmol) in THF (350 mL) was added under argon the BH_3 dimethylsulfide complex (42.7 mL, 450 mmol) at 50 °C over a period of 1 h. The reaction mixture was heated at reflux for 16 h. The excess borane was carefully destroyed by slow addition of MeOH at 25−35 °C. After multiple evaporations with MeOH, the residue was dissolved in 2 N aq. HCl (90 mL) and stirred at 80−90 °C for 0.5 h. The cold reaction mixture was extracted with *tert*-butylmethyl ether, and the aqueous phase was evaporated to dryness. Residual water was removed azeotropically with AcCN/toluene. The residual hydrochloride salt was dried under reduced pressure at 50 °C for 24 h to provide **56** (30.8 g, 99%) as a white solid, which was used without further purification. ^{1}H NMR (360 MHz, DMSO-d_6) δ 8.68 (s, 3H), 7.51−7.39 (m, 2H), 7.34−7.22 (m, 2H), 3.87−3.71 (m, 2H), 1.62 (s, 3H). MS *m*/*z* = 170 $[M + H]^+$.

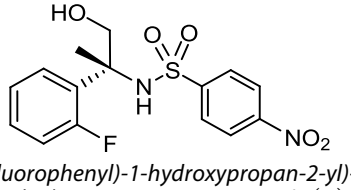

*(R)-N-(2-(2-Fluorophenyl)-1-hydroxypropan-2-yl)-4-nitrobenzenesulfonamide (**57**).* To a suspension of (*R*)-2-amino-2-(2-fluorophenyl)propan-1-ol hydrochloride (**56**) (4.05 g,19.6 mmol) in AcCN (25 mL) were added 4-methylmorpholine (5.4 mL, 49.1 mmol) and 4-nitrobenzene-1-sulfonyl chloride (4.87 g, 21.56 mmol) at 0−5 °C. The reaction mixture was stirred for 0.5 h at 0−5 °C and 2 h at 25 °C. The reaction was diluted with water (100 mL), and the AcCN was slowly removed under reduced pressure. The remaining water mixture was stirred for 1 h in an ice bath before the precipitated product was filtered off and washed with cold water and a small amount of Et_2O. The title compound **56** was obtained as a white solid (6.15 g, 88%) after drying under reduced pressure at 60 °C for 24 h and was used without further purification. ^{1}H NMR (400 MHz, $CDCl_3$-*d*) δ 8.12 (d, *J* = 8.6 Hz, 2H), 7.77 (d, *J* = 8.6 Hz, 2H), 7.34 (dd, *J* = 8.1, 1.5 Hz, 1H), 7.22−7.15 (m, 1H), 7.10 (td, *J* = 7.6, 1.4 Hz, 1H), 6.65 (ddd, *J* = 12.8, 8.1, 1.4 Hz, 1H), 5.57 (s, 1H), 4.26 (dd,

https://doi.org/10.1021/acs.jmedchem.0c02143
J. Med. Chem. 2021, 64, 4677−4696

J = 11.3, 5.4 Hz, 1H), 3.78 (dd, J = 11.3, 7.8 Hz, 1H), 2.17 (dd, J = 7.9, 5.6 Hz, 1H), 1.60 (s, 3 H). MS m/z = 372 $[M + NH_4]^+$.

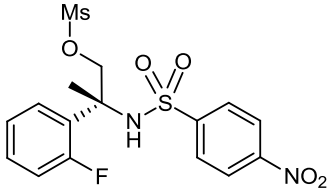

*(R)-2-(2-Fluorophenyl)-2-(4-nitrophenylsulfonamido)propyl Methanesulfonate (**58**).* To a suspension of (*R*)-*N*-(2-(2-fluorophenyl)-1-hydroxypropan-2-yl)-4-nitrobenzenesulfonamide (**57**) (5.7 g, 16 mmol) in AcCN (60 mL) were added 4-methylmorpholine (2.5 mL, 22.4 mmol) and a solution of methanesulfonyl chloride (1.62 mL, 20.8 mmol) in AcCN (5 mL) at 0−5 °C over a period of 20 min. After stirring for 0.5 h at 20 °C, the reaction mixture was poured onto ice-water and the AcCN was removed under reduced pressure. The aqueous phase was stirred for 1 h at 0−5 °C, and the crystallized product was filtered off. The residue was washed with Et_2O and dried under reduced pressure at 50 °C for 24 h to provide **58** (6.62 g, 95%) as a light-yellow solid. ^{1}H NMR (400 MHz, DMSO-d_6) δ 8.99 (s, 1H), 8.23−8.14 (m, 2H), 7.66−7.58 (m, 2H), 7.37 (td, J = 8.1, 1.8 Hz, 1H), 7.26−7.18 (m, 1H), 7.13 (td, J = 7.6, 1.3 Hz, 1H), 6.69 (ddd, J = 12.9, 8.1, 1.3 Hz, 1H), 4.67 (d, J = 9.7 Hz, 1H), 4.61 (d, J = 9.7 Hz, 1H), 3.24 (s, 3H), 1.67 (s, 3H). MS m/z = 337 $[M - MsOH]^+$.

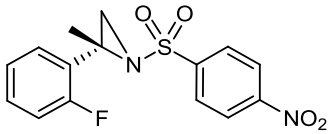

*(R)-2-(2-Fluorophenyl)-2-methyl-1-((4-nitrophenyl)sulfonyl)-aziridine (**59**). Method A.* To a solution of (*R*)-2-amino-2-(2-fluorophenyl)propan-1-ol hydrochloride (**56**) (200 mg, 0.875 mmol) in AcCN (5 mL) were added under argon 2-nitrobenzene-sulfonyl chloride (480 mg, 2.1 mmol) and $KHCO_3$ (442 mg, 4.38 mmol), and the reaction mixture was heated at reflux for 16 h. To accelerate the aziridine formation, Cs_2CO_3 (285 mg, 0.875 mmol) was added and the reaction mixture was heated for another 6 h at reflux. The reaction mixture was added to cold sat. aq. $NaHCO_3$ solution, and the product was extracted with EtOAc. Combined extracts were washed with water and brine, dried over $MgSO_4$, filtered, and concentrated. The residual oil was purified by flash chromatography on silica gel (hexane/EtOAc 10) to provide **59** (152 mg, 50%) as a yellow oil. ^{1}H NMR (360 MHz, $CDCl_3$) δ 8.33−8.28 (m, 2H), 8.14−8.09 (m, 2H), 7.38 (td, J = 7.6, 1.8 Hz, 1H), 7.26−7.19 (m, 1H), 7.07 (td, J = 7.5, 1.2 Hz, 1H), 6.96 (ddd, J = 10.5, 8.2, 1.2 Hz, 1H), 3.00 (s, 1H), 2.57 (s, 1H), 1.98 (s, 3H). MS m/z = 337 $[M + H]^+$.

Method B. To a suspension of (*R*)-*N*-(2-(2-fluorophenyl)-1-hydroxypropan-2-yl)-4-nitrobenzenesulfonamide (**57**) (5.0 g, 13.4 mmol) in CH_2Cl_2 (150 mL) were added at 0−5 °C NEt_3 (7.5 mL, 53.6 mmol) and at 0−5 °C a solution of methanesulfonyl chloride (2.1 mL, 26.8 mmol) in CH_2Cl_2 (10 mL). The reaction mixture was stirred for 0.5 h at 10−15 °C and for 2 h at 25−30 °C to complete aziridine formation and then poured onto cold 10% $Na_2H_2PO_4$ solution, and the product was extracted with EtOAc. Combined extracts were washed with water and brine, dried over $MgSO_4$, filtered, and concentrated. The crude product was crystallized from EtOAc/hexane to provide **58** (3.8 g, 84%) as a yellow solid. TLC (hexane/EtOAc 1:1) R_f = 0.66. ^{1}H NMR (360 MHz, $CDCl_3$) δ 8.33−8.28 (m, 2H), 8.14−8.09 (m, 2H), 7.38 (td, J = 7.6, 1.8 Hz, 1H), 7.26−7.19 (m, 1H), 7.07 (td, J = 7.5, 1.2 Hz, 1H), 6.96 (ddd, J = 10.5, 8.2, 1.2 Hz, 1H), 3.00 (s, 1H), 2.57 (s, 1H), 1.98 (s, 3H). MS m/z = 337 $[M + H]^+$.

Method C. To a solution of (*R*)-2-(2-fluorophenyl)-2-(4-nitrophenylsulfonamido)propyl methanesulfonate (**58**) (1.3 g, 3 mmol) in CH_2Cl_2 (30 mL) was added DBU (0.7 mL, 4.5 mmol) at 0−5 °C, and the reaction mixture was stirred for 2 h at 25 °C. The mixture was added to cold 10% $Na_2H_2PO_4$ solution, and the product was extracted with EtOAc. Combined extracts were washed with water and brine, dried over $MgSO_4$, filtered, and concentrated. The crude product was crystallized from EtOAc/hexane to provide **59** (0.74 g, 73%) as a yellow solid. TLC (hexane/EtOAc 1:1) R_f = 0.66. ^{1}H NMR (360 MHz, $CDCl_3$) δ 8.33−8.28 (m, 2H), 8.14−8.09 (m, 2H), 7.38 (td, J = 7.6, 1.8 Hz, 1H), 7.26−7.19 (m, 1H), 7.07 (td, J = 7.5, 1.2 Hz, 1H), 6.96 (ddd, J = 10.5, 8.2, 1.2 Hz, 1H), 3.00 (s, 1H), 2.57 (s, 1H), 1.98 (s, 3H). MS m/z = 337 $[M + H]^+$.

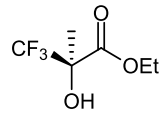

*(R)-Ethyl 3,3,3-Trifluoro-2-hydroxy-2-methylpropanoate (**39**).* To a solution of (*R*)-3,3,3-trifluoro-2-hydroxy-2-methylpropanoic acid (130.0 g, 822 mmol) in EtOH (420 mL) were added trimethylorthoformate (244.0 g, 1645 mmol) and H_2SO_4 (9.2 mL, 173 mmol), and the reaction mixture was heated at reflux for 50 h. The reaction mixture was reduced to half of its volume, and the remaining solution was added to sat. aq. $NaHCO_3$ solution (300 mL), and the product was extracted with *tert*-butylmethyl ether. Combined extracts were washed with brine, filtered, and concentrated under normal pressure. The residual oil was purified by vacuum distillation at 200 mbar (b.p. 88−90 °C) to provide **39** (131.4 g, 86%) as a colorless oil. ^{1}H NMR (400 MHz, $CDCl_3$) δ 4.44−4.26 (m, 2H), 3.82 (s, 1H), 1.58 (s, 3H), 1.34 (td, J = 7.1, 1.3 Hz, 3H).

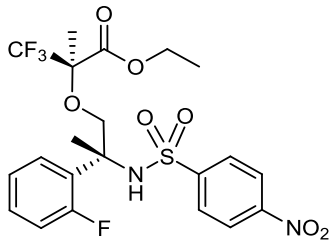

*(R)-Ethyl 3,3,3-Trifluoro-2-((R)-2-(2-fluorophenyl)-2-(4-nitrophenylsulfonamido)propoxy)-2-methylpropanoate (**60**). Method A.* To a solution of (*R*)-ethyl 3,3,3-trifluoro-2-hydroxy-2-methylpropanoate (**39**) (2.89 g, 15.5 mmol) in anhydrous DMF (20 mL) was added a 1 M solution of *tert*-butoxide in THF (15 mL, 15 mmol), and after 10 min of stirring, (*R*)-2-(2-fluorophenyl)-2-methyl-1-((4-nitrophenyl)sulfonyl)aziridine (**59**) (3.37 g, 10 mmol) was added at 35 °C and the reaction mixture was stirred for 6−10 h at 35 °C (monitored by HPLC). The reaction mixture was neutralized with 1 N aq. HCl at 0−5 °C to pH 7 and diluted with water (30 mL), and after stirring at 0−5 °C for 1 h, the precipitated product was collected and dried. Recrystallization from EtOAc-hexane gave **60** (4.54 g, 87%) as yellow crystals. ^{1}H NMR (400 MHz, $CDCl_3$) δ 8.24−8.19 (m, 2H), 7.92−7.83 (m, 2H), 7.66 (td, J = 8.1, 1.8 Hz, 1H), 7.29−7.23 (m, 1H), 7.19 (td, J = 7.6, 1.4 Hz, 1H), 6.86 (s, 1H), 6.76 (ddd, J = 12.7, 8.1, 1.4 Hz, 1H), 4.42 (qq, J = 10.7, 7.1 Hz, 2H), 3.82 (d, J = 8.9 Hz, 1H), 3.67 (d, J = 8.9 Hz, 1H), 1.62 (s, 3H), 1.60 (s, 3H), 1.40 (t, J = 7.1 Hz, 3H). MS m/z = 540 $[M + NH_4]^+$.

Method B. To a solution of (*R*)-2-(2-fluorophenyl)-2-(4-nitrophenylsulfonamido)propyl methanesulfonate (**58**) (4.0 g, 9.1 mmol) in anhydrous DMF (60 mL) were added under argon (*R*)-ethyl 3,3,3-trifluoro-2-hydroxy-2-methylpropanoate (**39**) (3.05 g, 16.38 mmol) and at 20−25 °C a 1 M solution of potassium *tert*-butoxide in THF (27.3 mL, 15 mmol). The reaction mixture was stirred for 30 min at 35 °C and then quenched by slow addition to cold 1 N aq. 1 N HCl, and the product was extracted with *tert*-butylmethyl ether. Combined extracts were washed with sat. aq. $NaHCO_3$ solution and brine, dried over $MgSO_4$, filtered, and concentrated. The crude product was recrystallized from EtOAc/diisopropylether/hexane to provide **69** (4.73 g, 72%) as a crystalline yellow solid. TLC (hexane/EtOAc 1:1) R_f =0.59. ^{1}H NMR (400 MHz, $CDCl_3$) δ 8.24−8.19 (m, 2H), 7.92−7.83 (m, 2H), 7.66 (td, J = 8.1, 1.8 Hz, 1H), 7.29−7.23 (m, 1H), 7.19 (td, J = 7.6, 1.4 Hz, 1H), 6.86 (s, 1H), 6.76 (ddd, J = 12.7, 8.1, 1.4 Hz, 1H), 4.42 (qq, J = 10.7, 7.1 Hz, 2H), 3.82 (d, J = 8.9 Hz, 1H), 3.67 (d, J = 8.9 Hz, 1H), 1.62

https://doi.org/10.1021/acs.jmedchem.0c02143
J. Med. Chem. 2021, 64, 4677−4696

(s, 3H), 1.60 (s, 3H), 1.40 (t, J = 7.1 Hz, 3H). MS m/z = 540 $[M + NH_4]^+$.

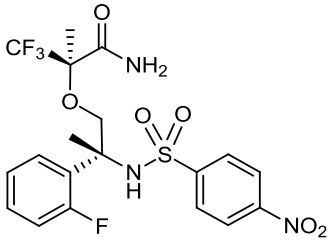

*(R)-3,3,3-Trifluoro-2-((R)-2-(2-fluorophenyl)-2-(4-nitrophenylsulfonamido)propoxy)-2-methylpropanamide (**61**).* A solution of (*R*)-ethyl 3,3,3-trifluoro-2-((*R*)-2-(2-fluorophenyl)-2-(4-nitrophenylsulfonamido)propoxy)-2-methylpropanoate (**60**) (4.5 g, 8.6 mmol) in 7 N NH_3 in MeOH was stirred in a sealed glass vessel at 50 °C for 36 h. The reaction mixture was concentrated, and the residual foam was dried under reduced pressure to afford the title compound **61** (4.4 g, 99%) as a yellow amorphous solid, which was used without further purification. ^{1}H NMR (400 MHz, DMSO-d_6) δ 8.85(s, 1H), 8.20 (d, J = 8.8 Hz, 2H), 7.91 (s, 1H), 7.73 (d, J = 8.8 Hz, 2H), 7.63 (s, 1H), 7.44 (td, J = 8.0, 1.8 Hz, 1H), 7.23 (m, 1H), 7.14 (td, J = 7.6, 1.4 Hz, 1H), 6.78 (m, 1H), 3.98 (d, J = 8.9 Hz, 1H), 3.72 (d, J = 8.9 Hz, 1H), 1.63 (s, 3H), 1.48 (s, 3H). MS m/z = 511 $[M + NH_4]^+$.

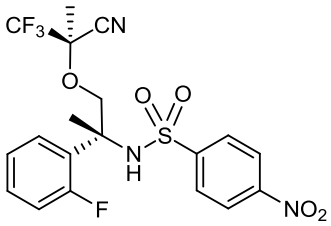

*N-((R)-1-(((R)-2-Cyano-1,1,1-trifluoropropan-2-yl)oxy)-2-(2-fluorophenyl)propan-2-yl)-4-nitrobenzenesulfonamide (**62**).* To a solution of (*R*)-3,3,3-trifluoro-2-((*R*)-2-(2-fluorophenyl)-2-(4-nitrophenylsulfonamido)propoxy)-2-methylpropanamide (**61**) (4.28 g, 8.5 mmol) and NEt_3 (2.96 mL, 21.25 mmol) in CH_2Cl_2 (50 mL) was added dropwise trifluoroacetic anhydride (1.45 mL, 10.2 mmol) over a period of 30 min. After stirring for 2 h at 0−5 °C, the reaction mixture was added to cold 5% aq. $NaHCO_3$ solution and the product was extracted with *tert*-butylmethyl ether. Combined extracts were washed with water, 0.1N aq. HCl, sat. aq. $NaHCO_3$ solution, and brine, dried over $MgSO_4$, filtered, and concentrated. The crude product was crystallized from EtOAc/heptane to provide the title compound **62** (3.85 g, 95%) as a white solid. ^{1}H NMR (400 MHz, DMSO-d_6) δ 8.87(s, 1H), 8.18 (d, J = 8.9 Hz, 2H), 7.65 (d, J = 8.8 Hz, 2H), 7.36 (td, J = 8.0, 1.8 Hz, 1H), 7.20 (m, 1H), 7.12 (td, J = 7.6, 1.4 Hz, 1H), 6.69 (m, 1H), 4.29 (d, J = 8.9 Hz, 1H), 4.09 (d, J = 8.9 Hz, 1H), 1.78 (s, 3H), 1.62 (s, 3H). MS m/z = 493 $[M + NH_4]^+$.

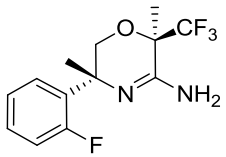

*(2R,5R)-5-(2-Fluorophenyl)-2,5-dimethyl-2-(trifluoromethyl)-5,6-dihydro-2H-1,4-oxazin-3-amine (**46**).* To a solution of *N*-((*R*)-1-(((*R*)-2-cyano-1,1,1-trifluoropropan-2-yl)oxy)-2-(2-fluorophenyl)-propan-2-yl)-4-nitrobenzenesulfonamide (**62**) (10.7 g, 22.5 mmol) in EtOH (70 mL) were added 2-acetamido-3-mercaptopropanoic acid (7.34 g, 45 mmol) and K_2CO_3 (6.84 g, 49.5 mmol), and the reaction mixture was heated at reflux for 72 h. The reaction mixture was concentrated to one-third of its volume and added to 10% aq. K_2CO_3 solution, and the product was extracted with *tert*-butylmethyl ether. Combined extracts were washed with brine, dried over $MgSO_4$, filtered through a plug of silica gel, and concentrated. The residual foam was dried under reduced pressure at 50 °C for 16 h to afford the title compound **46** (6.05 g, 92%) as a yellow amorphous solid, which was used without further purification. ^{1}H NMR (400 MHz, $CDCl_3$) δ 7.46 (td, J = 8.1, 1.9 Hz, 1H), 7.23 (ddt, J = 9.7, 4.9, 2.4 Hz, 1H), 7.10 (td, J = 7.6, 1.3 Hz, 1H), 7.02 (ddd, J = 12.4, 8.1, 1.3 Hz, 1H), 4.36 (br s, 2H), 4.07 (d, J = 11.7 Hz, 1H), 3.98−3.90 (m, 1H), 1.54 (d, J = 1.3 Hz, 3H), 1.46 (s, 3H). MS m/z = 291 $[M + H]^+$.

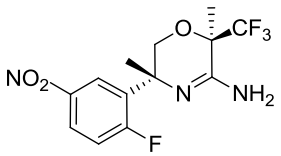

*(2R,5R)-5-(2-Fluoro-5-nitrophenyl)-2,5-dimethyl-2-(trifluoromethyl)-5,6-dihydro-2H-1,4-oxazin-3-amine (**50**).* To a solution of (2*R*,5*R*)-5-(2-fluorophenyl)-2,5-dimethyl-2-(trifluoromethyl)-5,6-dihydro-2*H*-1,4-oxazin-3-amine (**46**) (6.0 g, 20.6 mmol) in 98% sulfuric acid (40 mL) was added in portions KNO_3 (2.19 g, 21.65 mmol) at 0−5 °C over a period of 0.5 h, and the reaction mixture was stirred for 3 h at 22 °C. The reaction mixture was added to ice-water and was basified to pH 8−9 at 15−25 °C with 30% aq. NaOH. The product was extracted with EtOAc. Combined extracts were washed with brine, dried over $MgSO_4$, filtered, and concentrated. The crude product was purified by flash chromatography on silica gel (hexane/EtOAc 10:1 to 1:1) to provide the title compound **50** (5.62 g, 81%) as a light-yellow solid. TLC (toluene/EtOAc 3:1) R_f = 0.34. ^{1}H NMR (400 MHz, $CDCl_3$) δ 8.52 (dd, J = 6.7, 3.0 Hz, 1H), 8.15 (dt, J = 8.9, 3.6 Hz, 1H), 7.17 (dd, J = 10.6, 8.9 Hz, 1H), 4.76 (s, 2H), 4.06 (d, J = 11.6 Hz, 1H), 3.92 (d, J = 11.7 Hz, 1H), 1.56 (s, 3H), 1.49 (s, 3H). MS m/z = 336 $[M + H]^+$.

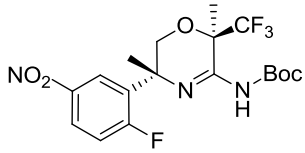

*tert-Butyl ((2R,5R)-5-(2-Fluoro-5-nitrophenyl)-2,5-dimethyl-2-(trifluoromethyl)-5,6-dihydro-2H-1,4-oxazin-3-yl)carbamate (**51**).* To a solution of (2*R*,5*R*)-5-(2-fluoro-5-nitrophenyl)-2,5-dimethyl-2-(trifluoromethyl)-5,6-dihydro-2*H*-1,4-oxazin-3-amine (**50**) (5.4 g, 15.9 mmol) in CH_2Cl_2 (100 mL) were added Boc_2O (4.5 g, 20.63 mmol) and NEt_3 (4.42 mL, 31.7 mmol), and the reaction mixture was stirred overnight at 22 °C. The reaction mixture was added to 10% aq. NaH_2PO_4 solution, and the product was extracted with CH_2Cl_2. Combined extracts were washed with water, dried over $MgSO_4$, filtered, and concentrated. The residue was crystallized from EtOAc/diisopropylether to provide the title compound **51** (6.38 g, 90%) as a light-yellow solid. TLC (hexane/EtOAc 3:1) R_f = 0.37. ^{1}H NMR (400 MHz, $CDCl_3$) δ 11.11 (s, 1H), 8.33−8.25 (m, 2H), 7.32 (t, J = 9.9 Hz, 1H), 4.43 (d, J = 12.4 Hz, 1H), 4.14 (d, J = 12.4 Hz, 1H), 1.73 (s, 3H), 1.57 (d, J = 1.9 Hz, 9H), 1.55 (s, 3H). MS m/z = 436 $[M + H]^+$.

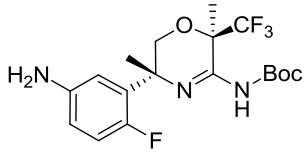

*tert-Butyl ((2R,5R)-5-(5-Amino-2-fluorophenyl)-2,5-dimethyl-2-(trifluoromethyl)-5,6-dihydro-2H-1,4-oxazin-3-yl)carbamate (**33b**).* A solution of *tert*-butyl ((2*R*,5*R*)-5-(2-fluoro-5-nitrophenyl)-2,5-dimethyl-2-(trifluoromethyl)-5,6-dihydro-2*H*-1,4-oxazin-3-yl)-carbamate (**51**) (6.2 g, 14.18 mmol) in dioxane (100 mL) was hydrogenated at atmospheric pressure with 5% Pd-C (1.5 g) for 3 h at 45 °C. The reaction mixture was filtered through Celite, and the filtrate was lyophilized. The white residue was recrystallized from *tert*-butylmethylether/hexane to provide the title compound **33b** (5.28 g, 92%) as a white solid. ^{1}H NMR (400 MHz, $CDCl_3$) δ 10.85 (s, 1H), 6.84 (dd, J = 11.8, 8.5 Hz, 1H), 6.60−6.48 (m, 2H), 4.32 (d, J = 12.1 Hz, 1H), 4.00 (d, J = 12.1 Hz, 1H), 3.62 (s, 2H), 1.61 (s, 3H), 1.51 (s, 3H), 1.49 (s, 9H). MS m/z = 406 $[M + H]^+$.

https://doi.org/10.1021/acs.jmedchem.0c02143
J. Med. Chem. 2021, 64, 4677−4696

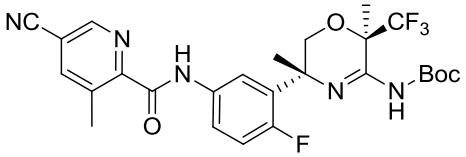

*tert-Butyl ((2R,5R)-5-(2-Fluoro-5-(5-cyano-3-methylpicolinamido)phenyl)-2,5-dimethyl-2-(trifluoromethyl)-5,6-dihydro-2H-1,4-oxazin-3-yl)carbamate (**53**).* To a solution of *tert*-butyl ((2*R*,5*R*)-5-(5-amino-2-fluorophenyl)-2,5-dimethyl-2-(trifluoromethyl)-5,6-dihydro-2*H*-1,4-oxazin-3-yl)carbamate (**33b**) (3.49 g, 8.6 mmol) in DMF (30 mL) were added at 0−5 °C 5-cyano-3-methylpicolinic acid (1.54 g, 9.46 mmol), EDC (1.74 g, 11.18 mmol), and HOAt (1.52 g, 11.18 mmol), and the reaction mixture was stirred overnight at 20 °C. The reaction mixture was added to sat. aq. $NaHCO_3$ solution, and the product was extracted with *tert*-butylmethylether. Combined extracts were washed with brine, dried over $MgSO_4$, filtered, and concentrated. The crude product was 2× recrystallized with diisopropylether to provide the title compound **53** (3.88 g, 81%) as a white crystalline solid. ^{1}H NMR (400 MHz, $CDCl_3$) δ 11.08−11.03 (m, 1H), 10.03 (s, 1H), 8.72 (d, J = 1.9 Hz, 1H), 7.95 (d, J = 1.8 Hz, 1H), 7.77 (dt, J = 8.5, 3.4 Hz, 1H), 7.61 (dd, J = 7.1, 2.6 Hz, 1H), 7.13 (dd, J = 11.5, 8.8 Hz, 1H), 4.42 (d, J = 12.2 Hz, 1H), 4.09 (d, J = 12.1 Hz, 1H), 2.85 (s, 3H), 1.70 (s, 3H), 1.59−1.53 (m, 12H). MS m/z = 550 $[M + H]^+$.

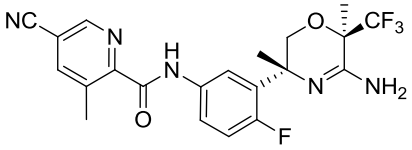

*N-(3-((3R,6R)-5-Amino-3,6-dimethyl-6-(trifluoromethyl)-3,6-dihydro-2H-1,4-oxazin-3-yl)-4-fluorophenyl)-5-cyano-3-methylpicolinamide (**54**).* To a solution of *tert*-butyl ((2*R*,5*R*)-5-(2-fluoro-5-(5-cyano-3-methylpicolinamido)phenyl)-2,5-dimethyl-2-(trifluoromethyl)-5,6-dihydro-2*H*-1,4-oxazin-3-yl)carbamate (**53**) (3.86 g, 7.0 mmol) in CH_2Cl_2 (30 mL) was added trifluoroacetic acid (5.1 mL, 70 mmol), and the reaction mixture was stirred for 2.5 h at 22 °C. The reaction mixture was added to excess 10% aq. $NaHCO_3$ solution, and the product was extracted with EtOAc. Combined extracts were washed with brine, dried over $MgSO_4$, filtered, and concentrated. The crude product was 2× recrystallized from *i*PrOH and dried at 50 °C for 24 h to provide the title compound **54** (2.64 g, 83%) as a colorless solid. M.p. 101−102 °C. TLC (CH_2Cl_2/MeOH 10:1) R_f =0.16. ^{1}H NMR (600 MHz, DMSO-d_6) δ 10.73 (s, 1H), 8.99 (s, 1H), 8.41 (s, 1H), 7.79 (dd, J = 7.4, 2.8 Hz, 1H), 7.72 (m, 1H), 7.16 (dd, J = 11.8, 8.7 Hz, 1H), 6.09 (s, 2H), 3.91 (d, J = 11.5 Hz, 1H), 3.81 (d, J = 11.4 Hz, 1H), 2.54 (s, 3H), 1.47 (s, 3H), 1.42 (s, 3H). ^{13}C NMR (151 MHz, DMSO-d_6) δ 163.74, 156.17 (d, $^1J_{CF}$ = 241.9 Hz), 153.68, 152.31, 148.78, 143.31, 134.19, 133.29 (d, $^2J_{CF}$ = 13.1 Hz), 133.14, 124.65 (q, $^1J_{CF}$ = 287.6 Hz), 121.93, 120.66 ($^3J_{CF}$ = 8.5 Hz), 116.58, 115.99 (d, $^2J_{CF}$ = 25.2 Hz), 110.03, 72.07 (q, $^2J_{CF}$ = 27.2 Hz), 67.27, 54.97, 25.63, 18.53, 18.29. ^{19}F NMR (376 MHz, DMSO-d_6) δ −74.67 (s, 3F), −117.10 (s, 1F). HRMS (ESI+): m/z calcd for $C_{21}H_{19}N_5O_2F_4$ $[M + H]^+$ 450.15476, found 450.15485.

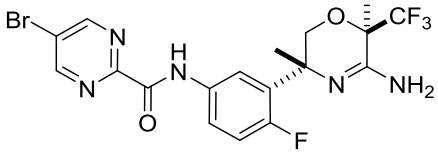

*N-(3-((3R,6R)-5-Amino-3,6-dimethyl-6-(trifluoromethyl)-3,6-dihydro-2H-1,4-oxazin-3-yl)-4-fluorophenyl)-5-bromopyrimidine-2-carboxamide Hydrochloride (**64a**).* **64a** was obtained according to the procedure described for compounds **53** and **38a** starting from **33b** and 5-bromopyrimidine-2-carboxylic acid (**63a**) as an off-white solid (85, 88%). ^{1}H NMR (600 MHz, DMSO-d_6) δ 11.7 (s, 1H), 11.1 (s, 1H), 9.61 (s, 2H), 9.32 (s, 2H), 7.99 (m, 1H), 7.93 (d, J = 3.2 Hz, 1H), 7.36 (dd, J = 11.8, 8.7 Hz, 1H), 4.34 (d, J = 11.5 Hz, 1H), 4.08 (d, J = 11.4 Hz, 1H), 1.65 (s, 3H), 1.59 (s, 3H). MS m/z = 490/492 $[M + H]^+$. HRMS (ESI+): m/z calcd for $C_{18}H_{17}N_5O_2BrF_4$ $[M + H]^+$ 490.04963, found 490.04965.

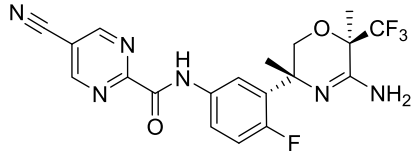

rac-N-(3-((3R,6R*)-5-Amino-3,6-dimethyl-6-(trifluoromethyl)-3,6-dihydro-2H-1,4-oxazin-3-yl)-4-fluorophenyl)-5-cyanopyrimidine-2-carboxamide Trifluoroacetate (rac-**64b**).* ***rac*-64b** was obtained according to the procedure described for compounds **53** and **54** starting from *rac*-**33b** and 5-cyano-3-methylpyrazine-2-carboxylic acid (**63b**) as an off-white solid (16, 94%). ^{1}H NMR (400 MHz, $CDCl_3$) δ 11.16 (s, 1H), 9.95 (s, 1H), 9.18 (s, 2H), 8.96 (s, 2H), 7.95−7.87 (m, 1H), 7.57−7.49 (m, 1H), 7.10 (dd, J = 11.5, 8.7 Hz, 1H), 4.45 (d, J = 12.5 Hz, 1H), 4.01 (d, J = 12.5 Hz, 1H), 1.73 (s, 3H), 1.67 (s, 3H). MS m/z = 437 $[M + H]^+$.

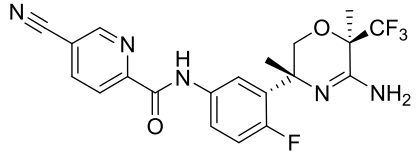

*N-(3-((3R,6R)-5-Amino-3,6-dimethyl-6-(trifluoromethyl)-3,6-dihydro-2H-1,4-oxazin-3-yl)-4-fluoro-phenyl)-5-cyanopicolinamide Hydrochloride (**64c**).* **64c** was obtained according to the procedure described for compounds **53** and **54** starting from **33b** and 5-cyano-3-methylpyrazine-2-carboxylic acid (**63c**) as an off-white solid (86, 91%). ^{1}H NMR (400 MHz, DMSO-d_6) δ 10.85 (s, 1H), 9.26−9.10 (m, 1H), 8.56 (dd, J = 8.2, 2.2 Hz, 1H), 8.32−8.16 (m, 1H), 7.93 (dd, J = 7.4, 2.7 Hz, 1H), 7.84−7.62 (m, 1H), 7.16 (dd, J = 11.8, 8.9 Hz, 1H), 6,25 (br s, 2H), 3.94 (d, J = 11.5 Hz, 1H), 4.81 (d, J = 11.6 Hz, 1H), 1.49 (s, 3H), 1.43 (s, 3H). HRMS (ESI+): m/z calcd for $C_{20}H_{18}N_5O_2F_4$ $[M + H]^+$ 436.13911, found 436.13904.

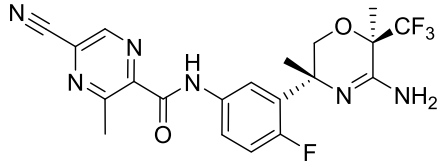

*N-(3-((3R,6R)-5-Amino-3,6-dimethyl-6-(trifluoromethyl)-3,6-dihydro-2H-1,4-oxazin-3-yl)-4-fluorophenyl)-5-cyano-3-methylpyrazine-2-carboxamide (**64d**).* **64d** was obtained according to the procedure described for compounds **53** and **54** starting from **33b** and 5-cyano-3-methylpyrazine-2-carboxylic acid (**63d**) as an off-white solid (55, 79%). ^{1}H NMR (400 MHz, MeOD-d_4) δ 9.01 (s, 1H), 7.86 (dd, J = 7.4, 2.8 Hz, 1H), 7.74 (m, 1H), 7.20 (dd, J = 11.8, 7.7 Hz, 1H), 4.19 (d, J = 11.5 Hz, 1H), 3.35 (d, J = 11.4 Hz, 1H), 2.93 (s, 3H), 1.57 (s, 3H), 1.32 (s, 3H). HRMS (ESI+): m/z calcd for $C_{20}H_{19}N_6O_2F_4$ $[M + H]^+$ 451.15001, found 451.15018.

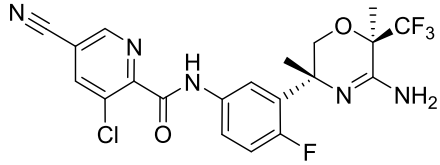

*N-(3-((3R,6R)-5-Amino-3,6-dimethyl-6-(trifluoromethyl)-3,6-dihydro-2H-1,4-oxazin-3-yl)-4-fluorophenyl)-3-chloro-5-cyanopicolinamide Hydrochloride (**64e**).* **64e** was obtained according to the procedure described for compounds **53** and **54** starting from **33b** and 3-chloro-5-cyanopicolinic acid (**63e**) as a white solid (81, 95%). ^{1}H NMR (600 MHz, DMSO-d_6) δ 10.92 (s, sH), 9.12 (d, J = 1.5 Hz, 1H), 8.82 (d, J = 1.5 Hz, 1H), 7.71 (d, J = 5.7 Hz, 2H), 7.25−7.08 (m, 1H), 6.11 (s, 2H), 3.93 (d, J = 11.5 Hz, 1H), 3.79 (d, J = 11.4 Hz, 1H), 1.46 (s, 3H), 1.42 (s, 3H). HRMS (ESI+): m/z calcd for $C_{20}H_{17}N_5O_2ClF_4$ $[M + H]^+$ 470.10014, found 470.10043.

https://doi.org/10.1021/acs.jmedchem.0c02143
J. Med. Chem. 2021, 64, 4677−4696

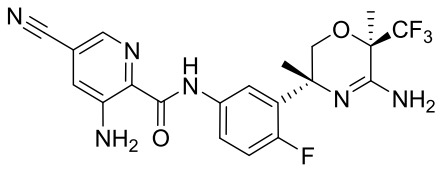

*3-Amino-N-(3-((3R,6R)-5-amino-3,6-dimethyl-6-(trifluoromethyl)-3,6-dihydro-2H-1,4-oxazin-3-yl)-4-fluorophenyl)-5-cyanopicolinamide (**64f**).* **64f** was obtained according to the procedure described for compounds **53** and **54** starting from **33b** and 3-amino-5-cyanopicolinic acid (**63f**) as a light-yellow foam (53, 77%). ^{1}H NMR (600 MHz, DMSO-d_6) δ 10.51 (s, 1H), 8.21 (s, 1 H), 7.84 (m, 1H), 7.69 (m, 1H), 7.63 (s, 1H), 7.24 (s, 2H), 7.13 (dd, J = 11.2, 7.6 Hz, 1H), 6.08 (s, 1H), 3.80−3.92 (m, 2H), 1.48 (s, 3H), 1.39 (s, 3H). HRMS (ESI+): m/z calcd for $C_{18}H_{17}N_5O_2BrF_4$ $[M + H]^+$ 451.15001, found 451.15012.

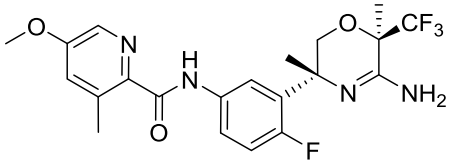

*N-(3-((3R,6R)-5-Amino-3,6-dimethyl-6-(trifluoromethyl)-3,6-dihydro-2H-1,4-oxazin-3-yl)-4-fluorophenyl)-5-methoxy-3-methylpicolinamide (**64g**).* **64g** was obtained according to the procedure described for compounds **53** and **54** starting from **33b** and 5-methoxy-3-methylpicolinic acid (**63g**) as a light-yellow foam (62, 94%). ^{1}H NMR (400 MHz, DMSO-d_6) δ 11.54 (s, 1H), 10.67 (s, 1H), 9.55 (m, 2H), 8.24 (d, J = 2.5 Hz, 1H), 7.98 (m, 1H), 7.89 (dd, J = 7.7, 2.4 Hz, 1H), 7.43 (d, J = 3.3 Hz, 1H), 7.30 (dd, J = 12.1, 8.8 Hz, 1H), 4.31 (d, J = 12.6 Hz, 1H), 4.07 (d, J = 12.8 Hz, 1H), 3.91 (s, 3H), 2.62 (s, 3H), 1.76 (s, 3H), 1.72 (s, 3H). HRMS (ESI+): m/z calcd for $C_{21}H_{23}N_4O_3F_4$ $[M + H]^+$ 455.17008, found 455.17020.

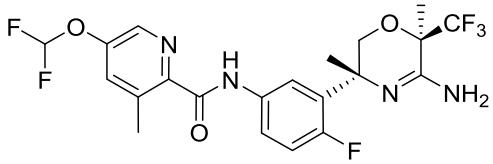

*N-(3-((3R,6R)-5-Amino-3,6-dimethyl-6-(trifluoromethyl)-3,6-dihydro-2H-1,4-oxazin-3-yl)-4-fluorophenyl)-5-(difluoromethoxy)-3-methylpicolinamide Hydrochloride (**64h**).* **64h** was obtained according to the procedure described for compounds **53** and **54** starting from **33b** and 5-(difluoromethoxy)-3-methylpicolinic acid (**63h**) as a light-yellow foam (76, 62%). ^{1}H NMR (400 MHz, DMSO-d_6) δ 11.53 (s, 1H), 10.78 (s, 1H), 9.54 (m, 2H), 8.45 (d, J = 2.5 Hz, 1H), 7.97 (m, 1H), 7.88 (dd, J = 7.5, 2.5 Hz, 1H), 7.75 (d, J = 2.3 Hz, 1H), 7.45 (t, 1H), 7.32 (dd, J = 12.1, 8.8 Hz, 1H), 4.32 (d, J = 12.6 Hz, 1H), 4.08 (d, J = 12.6 Hz, 1H), 2.60 (s, 3H), 1.75 (s, 3H), 1.72 (s, 3H). HRMS (ESI+): m/z calcd for $C_{21}H_{21}N_4O_3F_6$ $[M + H]^+$ 491.15124, found 491.15131.

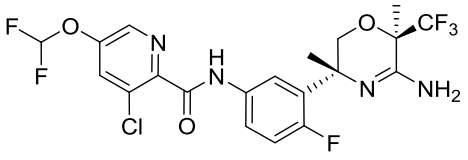

*N-(3-((3R,6R)-5-Amino-3,6-dimethyl-6-(trifluoromethyl)-3,6-dihydro-2H-1,4-oxazin-3-yl)-4-fluorophenyl)-3-chloro-5-(difluoromethoxy)picolinamide (**64i**).* **64i** was obtained according to the procedure described for compounds **53** and **54** starting from **33b** and 3-chloro-5-(difluoromethoxy)picolinic acid (**63i**) as a white solid (92, 86%). ^{1}H NMR (600 MHz, DMSO-d_6) δ 10.74 (s, 1H), 8.59 (d, J = 2.3 Hz, 1H), 8.13 (d, J = 2.3 Hz, 1H), 7.74 (dd, J = 7.3, 2.7 Hz, 1H), 7.72−7.66 (m, 1H), 7.50 (t, J = 72.7 Hz, 1H), 7.17 (dd, J = 11.7, 8.8 Hz, 1H), 6.10 (s, 2H), 3.93 (d, J = 11.5 Hz, 1H), 3.79 (d, J = 11.5 Hz, 1H), 1.47 (s, 3H), 1.42 (s, 3H). HRMS (ESI+): m/z calcd for $C_{20}H_{18}N_4O_3ClF_6$ $[M + H]^+$ 511.09661, found 511.09677.

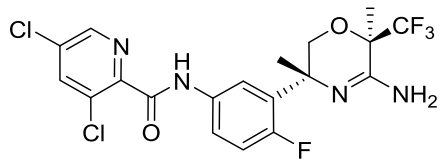

*N-(3-((3R,6R)-5-Amino-3,6-dimethyl-6-(trifluoromethyl)-3,6-dihydro-2H-1,4-oxazin-3-yl)-4-fluorophenyl)-3,5-dichloropicolinamide Hydrochloride (**64j**).* **64j** was obtained according to the procedure described for compounds **53** and **54** starting from **33b** and 3,5-dichloropicolinic acid (**63j**) as a white solid (90, 88%). ^{1}H NMR (400 MHz, DMSO-d_6) δ 10.72 (s, 1H), 8.87−8.64 (m, 1H), 8.43 (d, J = 1.9 Hz, 1H), 7.84−7.59 (m, 2H), 7.29−7.04 (m, 1H), 6.05 (br s, 2H), 3.91 (d, J = 11.7 Hz, 1H), 3.77 (d, J = 11.3 Hz, 1H), 1.45 (s, 3H), 1.40 (s, 3H). HRMS (ESI+): m/z calcd for $C_{19}H_{17}N_4O_2Cl_2F_4$ $[M + H]^+$ 479.06592, found 479.06598.

■ ASSOCIATED CONTENT

Supporting Information

The Supporting Information is available free of charge at https://pubs.acs.org/doi/10.1021/acs.jmedchem.0c02143.

Preparation details and analytical data for compounds **4**, *rac*-**20**, *rac*-(3*R**,6*R**)-**38a−d**, *rac*-(3*R**,6*S**)-**38e**, *rac*-**49**, and **50** (PDF)

Molecular formula strings and some data (CSV)

Accession Codes

Crystal structure coordinates and structure factors have been deposited in the Protein Data Bank (PDB) with the accession codes 7B1E (**3**), 7B1P (**38a**), and 7B1Q (**54**). Authors will release the atomic coordinates and experimental data upon article publication.

■ AUTHOR INFORMATION

Corresponding Author

Rainer Machauer − *Global Discovery Chemistry, Novartis Institutes for BioMedical Research, Novartis Pharma AG, CH-4057 Basel, Switzerland;* orcid.org/0000-0001-5081-6268; Email: rainer.machauer@novartis.com

Authors

Heinrich Rueeger − *Global Discovery Chemistry, Novartis Institutes for BioMedical Research, Novartis Pharma AG, CH-4057 Basel, Switzerland*

Rainer Lueoend − *Global Discovery Chemistry, Novartis Institutes for BioMedical Research, Novartis Pharma AG, CH-4057 Basel, Switzerland*

Siem J. Veenstra − *Global Discovery Chemistry, Novartis Institutes for BioMedical Research, Novartis Pharma AG, CH-4057 Basel, Switzerland*

Philipp Holzer − *Global Discovery Chemistry, Novartis Institutes for BioMedical Research, Novartis Pharma AG, CH-4057 Basel, Switzerland*

Konstanze Hurth − *Global Discovery Chemistry, Novartis Institutes for BioMedical Research, Novartis Pharma AG, CH-4057 Basel, Switzerland*

Markus Voegtle − *Global Discovery Chemistry, Novartis Institutes for BioMedical Research, Novartis Pharma AG, CH-4057 Basel, Switzerland*

Mathias Frederiksen − *Global Discovery Chemistry, Novartis Institutes for BioMedical Research, Novartis Pharma AG, CH-4057 Basel, Switzerland*

Jean-Michel Rondeau − *Center for Proteomic Chemistry, Structural Biology Platform, Novartis Institutes for*

BioMedical Research, Novartis Pharma AG, CH-4057 Basel, Switzerland

Marina Tintelnot-Blomley − *Global Discovery Chemistry, Novartis Institutes for BioMedical Research, Novartis Pharma AG, CH-4057 Basel, Switzerland*

Laura H. Jacobson − *Department of Neuroscience, Novartis Institutes for BioMedical Research, Novartis Pharma AG, CH-4057 Basel, Switzerland*

Matthias Staufenbiel − *Department of Neuroscience, Novartis Institutes for BioMedical Research, Novartis Pharma AG, CH-4057 Basel, Switzerland*

Grit Laue − *Metabolism and Pharmacokinetics, Novartis Institutes for BioMedical Research, Novartis Pharma AG, CH-4057 Basel, Switzerland*

Ulf Neumann − *Department of Neuroscience, Novartis Institutes for BioMedical Research, Novartis Pharma AG, CH-4057 Basel, Switzerland*

Complete contact information is available at: https://pubs.acs.org/10.1021/acs.jmedchem.0c02143

Author Contributions

The manuscript was written through contributions of all authors. All authors have given approval to the final version of the manuscript.

Notes

The authors declare the following competing financial interest(s): H.R., R.L., R.M., S.J.V., P.H., K.H., M.V., M.F., J.-M.R., M.T.-B., L.H.J., M.S., G.L. and U.N. are current or former employees of Novartis Pharma AG, which has a commercial interest to develop BACE1 inhibitors.

■ ACKNOWLEDGMENTS

We thank K. Barker, M. Furegati, C. Hartwieg, M. Hediger, S. Jacquier, P. Koeninger, C. Rolando, T. Ruppen, H. Schütz, U. Stauss, M. Vogt, J. Zadrobilek, and T. Zimmermann for synthetic support; T. Dittmar, V. Trappe, I. Brzak, L. Perrot, and U. Furrer for *in vitro* and *in vivo* studies; K. Beltz and R. Ramos for compound formulation support; S. Lehmann and E. Wirth for X-ray support; and R. Hemmig for the preparation of refolded BACE1. We are grateful to the machine and beamline groups at the Paul Scherrer Institute, Villigen, Switzerland, for the X-ray data collection of the BACE1 complexes with compounds **3** and **54**.

■ ABBREVIATIONS USED

aq., aqueous; AUC, area under the curve; BACE, β-site APP-cleaving enzyme; Boc, butyloxycarbonyl; *t*-BuOK, potassium *tert*-butoxide; CL, clearance; CSF, cerebrospinal fluid; CNS, central nervous system; CYP, cytochrome P450 enzyme; DME, 1,2-dimethoxyethane; DBU, 1,8-diazabicycloundec-7-ene; DIPEA, *N*,*N*-diisopropylethylamine; DMF, *N*,*N*-dimethylformamide; DMSO, dimethyl sulfoxide; EDC, 1-ethyl-3-(3-dimethylaminopropyl)carbodiimide; ee, enantiomeric excess; eq., equivalent; Et_2O, diethylether; EtOAc, ethyl acetate; EtOH, ethanol; ER, efflux ratio; hERG, human ether-a-go-go related gene; HOAt, 1-hydroxy-7-azabenzotriazole; iPrOH, *iso*-propanol; LC, liquid chromatography; MDCK, Madin−Darby canine kidney; MDR1, multidrug-resistance gene 1; MeOH, methanol; MS, mass spectrospopy; Ms, methanesulfonyl; Ms-Cl, methanesulfonyl chloride; NaOAc, sodium acetate; NMM, *N*-methylmorpholine; NMP, *N*-methyl-2-pyrrolidone; Ns, nosyl; Ns-Cl, nosyl chloride; PEG, poly(ethylene glycol); *i*-PrOH, 2-propanol; PD, pharmacodynamics; PK, pharmacokinetic; SAR, structure−activity relationship; sat., saturated; SFC, chiral supercritical fluid chromatography; THF, tetrahydrofuran; TFA, trifluoroacetic acid; TFAA, trifluoroacetic anhydride; V_{ss}, volume of distribution

■ REFERENCES

(1) Ising, C.; Stanley, M.; Holtzman, D. M. Current thinking on the mechanistic basis of Alzheimer's and implications for drug development. *Clin. Pharmacol. Ther.* **2015**, *98*, 469−471.

(2) Heneka, M. T.; Carson, M. J.; Khoury, J. E.; Landreth, G. E.; Brosseron, F.; Feinstein, D. L.; Jacobs, A. H.; Wyss-Coray, T.; Vitorica, J.; Ransohoff, R. M.; Herrup, K.; Frautschy, S. A.; Finsen, B.; Brown, G. C.; Verkhratsky, A.; Yamanaka, K.; Koistinaho, J.; Latz, E.; Halle, A.; Petzold, G. C.; Town, T.; Morgan, D.; Shinohara, M. L.; Perry, V. H.; Holmes, C.; Bazan, N. G.; Brooks, D. J.; Hunot, S.; Joseph, B.; Deigendesch, N.; Garaschuk, O.; Boddeke, E.; Dinarello, C. A.; Breitner, J. C.; Cole, G. M.; Golenbock, D. T.; Kummer, M. P. Neuroinflammation in Alzheimer's disease. *Lancet Neurol.* **2015**, *14*, 388−405.

(3) Villemagne, V. L.; Pike, K. E.; Chetelat, G.; Ellis, K. A.; Mulligan, R. S.; Bourgeat, P.; Ackermann, U.; Jones, G.; Szoeke, C.; Salvado, O.; Martins, R.; O'Keefe, G.; Mathis, C. A.; Klunk, W. E.; Ames, D.; Masters, C. L.; Rowe, C. C. Longitudinal assessment of Aβ and cognition in aging and Alzheimer disease. *Ann. Neurol.* **2011**, *69*, 181−192.

(4) Villemagne, V. L.; Burnham, S.; Bourgeat, P.; Brown, B.; Ellis, K. A.; Salvado, O.; Szoeke, C.; Macaulay, S. L.; Martins, R.; Maruff, P.; Ames, D.; Rowe, C. C.; Masters, C. L. Amyloid beta deposition, neurodegeneration, and cognitive decline in sporadic Alzheimer's disease: a prospective cohort study. *Lancet Neurol.* **2013**, *12*, 357−367.

(5) Jack, C. R., Jr.; Knopman, D. S.; Jagust, W. J.; Shaw, L. M.; Aisen, P. S.; Weiner, M. W.; Petersen, R. C.; Trojanowski, J. Q. Hypothetical model of dynamic biomarkers of the Alzheimer's pathological cascade. *Lancet Neurol.* **2010**, *9*, 119−128.

(6) Sperling, R.; Mormino, E.; Johnson, K. The evolution of preclinical Alzheimer's disease: implications for prevention trials. *Neuron* **2014**, *84*, 608−622.

(7) Siemers, E. R.; Sundell, K. L.; Carlson, C.; Case, M.; Sethuraman, G.; Liu-Seifert, H.; et al. Phase 3 solanezumab trials: secondary outcomes in mild Alzheimer's disease patients. *Alzheimer's Dementia* **2016**, *12*, 110−120.

(8) Masters, C. L.; Selkoe, D. J. Biochemistry of amyloid beta-protein and amyloid deposits in Alzheimer disease. *Cold Spring Harbor Perspect. Med.* **2012**, *2*, No. a006262.

(9) Selkoe, D. J. Resolving controversies on the path to Alzheimer's therapeutics. *Nat. Med.* **2011**, *17*, 1060−1065.

(10) Abramowski, D.; Wiederhold, K. H.; Furrer, U.; Jaton, A. L.; Neuenschwander, A.; Runser, M. J.; Danner, S.; Reichwald, J.; Ammaturo, D.; Staab, D.; Stoeckli, M.; Rueeger, H.; Neumann, U.; Staufenbiel, M. Dynamics of Abeta turnover and deposition in different beta-amyloid precursor protein transgenic mouse models following gamma-secretase inhibition. *J. Pharmacol. Exp. Ther.* **2008**, *327*, 411−424.

(11) Rabe, S.; Reichwald, J.; Ammaturo, D.; de Strooper, B.; Saftig, P.; Neumann, U.; Staufenbiel, M. The Swedish APP mutation alters the effect of genetically reduced BACE1 expression on the APP processing. *J. Neurochem.* **2011**, *119*, 231−239.

(12) McConlogue, L.; Buttini, M.; Anderson, J. P.; Brigham, E. F.; Chen, K. S.; Freedman, S. B.; Games, D.; Johnson-Wood, K.; Lee, M.; Zeller, M.; Liu, W.; Motter, R.; Sinha, S. Partial reduction of BACE1 has dramatic effects on Alzheimer plaque and synaptic pathology in APP transgenic mice. *J. Biol. Chem.* **2007**, *282*, 26326−26334.

(13) Ostermann, N.; Eder, J.; Eidhoff, U.; Zink, F.; Hassiepen, U.; Worpenberg, S.; Maibaum, J.; Simic, O.; Hommel, U.; Gerhartz, B. Crystal structure of human BACE2 in complex with a hydroxyethylamine transition-state inhibitor. *J. Mol. Biol.* **2006**, *355*, 249−261.

(14) Willem, M.; Garratt, A. N.; Novak, B.; Citron, M.; Kaufmann, S.; Rittger, A.; DeStrooper, B.; Saftig, P.; Birchmeier, C.; Haass, C. Control of peripheral nerve myelination by the beta-secretase BACE1. *Science* **2006**, *314*, 664−676.
(15) Velanac, V.; Unterbarnscheidt, T.; Hinrichs, W.; Gummert, M. N.; Fischer, T. M.; Rossner, M. J.; Trimarco, A.; Brivio, V.; Taveggia, C.; Willem, M.; Haass, C.; Mobius, W.; Nave, K. A.; Schwab, M. H. Bace1 processing of NRG1 type III produces a myelin-inducing signal but is not essential for the stimulation of myelination. *Glia* **2012**, *60*, 203−217.
(16) Eggert, S.; Paliga, K.; Soba, P.; Evin, G.; Masters, C. L.; Weidemann, A.; Beyreuther, K. The proteolytic processing of the amyloid precursor protein gene family members APLP-1 and APLP-2 involves alpha-, beta-, gamma-, and epsilon-like cleavages: modulation of APLP-1 processing by n-glycosylation. *J. Biol. Chem.* **2004**, *279*, 18146−18156.
(17) Barão, S.; Gärtner, A.; Leyva-Díaz, E.; Demyanenko, G.; Munck, S.; Vanhoutvin, T.; Zhou, L.; Schachner, M.; López-Bendito, G.; Maness, P. F.; De Strooper, B. , Patricia, F.;, B. Antagonistic effects of BACE1 and APH1B-γ-secretase control axonal guidance by regulating growth cone collapse. *Cell Rep.* **2015**, *12*, 1367−1376.
(18) Kuhn, P. H.; Koroniak, K.; Hogl, S.; Colombo, A.; Zeitschel, U.; Willem, M.; Volbracht, C.; Schepers, U.; Imhof, A.; Hoffmeister, A.; Haass, C.; Rossner, S.; Brase, S.; Lichtenthaler, S. F. Secretome protein enrichment identifies physiological BACE1 protease substrates in neurons. *EMBO J.* **2012**, *31*, 3157−3168.
(19) Wessels, A. M.; Lines, C.; Stern, R. A.; Kost, J.; Voss, T.; Mozley, L. H.; Furtek, C.; Mukai, Y.; Aisen, P. S.; Cummings, J. L.; Tariot, P. N.; Vellas, B.; Dupre, N.; Randolph, C.; Michelson, D.; Andersen, S. W.; Shering, C.; Sims, J. R.; Egan, M. F. Cognitive outcomes in trials of two BACE inhibitors in Alzheimer's disease. *Alzheimer's Dementia* **2020**, *16*, 1483−1492.
(20) Ghosh, A. K.; Osswald, H. L. BACE1 (beta-secretase) inhibitors for the treatment of Alzheimer's disease. *Chem. Soc. Rev.* **2014**, *43*, 6765−6813.
(21) Yuan, J.; Venkatraman, S.; Zheng, Y.; McKeever, B. M.; Dillard, L. W.; Singh, S. B. Structure-based design of beta-site APP cleaving enzyme 1 (BACE1) inhibitors for the treatment of Alzheimer's disease. *J. Med. Chem.* **2013**, *56*, 4156−4180.
(22) Wager, T. T.; Villalobos, A.; Verhoest, P. R.; Hou, X.; Shaffer, C. L. Strategies to optimize the brain availability of central nervous system drug candidates. *Expert Opin. Drug Discovery* **2011**, *6*, 371−381.
(23) Wager, T. T.; Chandrasekaran, R. Y.; Hou, X.; Troutman, M. D.; Verhoest, P. R.; Villalobos, A.; Will, Y. Defining desirable central nervous system drug space through the alignment of molecular properties, in vitro ADME, and safety attributes. *ACS Chem. Neurosci.* **2010**, *1*, 420−434.
(24) Feng, B.; Mills, J. B.; Davidson, R. E.; Mireles, R. J.; Janiszewski, J. S.; Troutman, M. D.; de Morais, S. M. In vitro P-glycoprotein assays to predict the in vivo interactions of P-glycoprotein with drugs in the central nervous system. *Drug Metab. Dispos.* **2008**, *36*, 268−275.
(25) Doran, A.; Obach, R. S.; Smith, B. J.; Hosea, N. A.; Becker, S.; Callegari, E.; Chen, C.; Chen, X.; Choo, E.; Cianfrogna, J.; Cox, L. M.; Gibbs, J. P.; Gibbs, M. A.; Hatch, H.; Hop, C. E.; Kasman, I. N.; Laperle, J.; Liu, J.; Liu, X.; Logman, M.; Maclin, D.; Nedza, F. M.; Nelson, F.; Olson, E.; Rahematpura, S.; Raunig, D.; Rogers, S.; Schmidt, K.; Spracklin, D. K.; Szewc, M.; Troutman, M.; Tseng, E.; Tu, M.; Van Deusen, J. W.; Venkatakrishnan, K.; Walens, G.; Wang, E. Q.; Wong, D.; Yasgar, A. S.; Zhang, C. The impact of P-glycoprotein on the disposition of drugs targeted for indications of the central nervous system: evaluation using the MDR1A/1B knockout mouse model. *Drug Metab. Dispos.* **2005**, *33*, 165−174.
(26) Raub, T. J. P-glycoprotein recognition of substrates and circumvention through rational drug design. *Mol. Pharmceutics* **2006**, *3*, 3−25.
(27) Mahar Doan, K. M.; Humphreys, J. E.; Webster, L. O.; Wring, S. A.; Shampine, L. J.; Serabjit-Singh, C. J.; Adkison, K. K.; Polli, J. W. Passive permeability and P-glycoprotein-mediated efflux differentiate central nervous system (CNS) and non-CNS marketed drugs. *J. Pharmacol. Exp. Ther.* **2002**, *303*, 1029−1037.
(28) Hitchcock, S. A. Structural modifications that alter the P-glycoprotein efflux properties of compounds. *J. Med. Chem.* **2012**, *55*, 4877−4895.
(29) Didziapetris, R.; Japertas, P.; Avdeef, A.; Petrauskas, A. Classification analysis of P-glycoprotein substrate specificity. *J. Drug Targeting* **2003**, *11*, 391−406.
(30) Norinder, U.; Haeberlein, M. Computational approaches to the prediction of the blood-brain distribution. *Adv. Drug Delivery Rev.* **2002**, *54*, 291−313.
(31) Clark, D. E. Rapid calculation of polar molecular surface area and its application to the prediction of transport phenomena. 1. prediction of intestinal absorption. *J. Pharm. Sci.* **1999**, *88*, 807−814.
(32) Aronov, A. M. Ligand structural aspects of hERG channel blockade. *Curr. Top. Med. Chem.* **2008**, *8*, 1113−1127.
(33) Rueeger, H.; Lueoend, R.; Rogel, O.; Rondeau, J. M.; Möbitz, H.; Machauer, R.; Jacobson, L.; Staufenbiel, M.; Desrayaud, S.; Neumann, U. Discovery of cyclic sulfone hydroxyethylamines as potent and selective beta-site APP-cleaving enzyme 1 (BACE1) inhibitors: structure-based design and in vivo reduction of amyloid beta-peptides. *J. Med. Chem.* **2012**, *55*, 3364−3386.
(34) Rueeger, H.; Lueoend, R.; Machauer, R.; Veenstra, S. J.; Jacobson, L. H.; Staufenbiel, M.; Desrayaud, S.; Rondeau, J.-M.; Möbitz, H.; Neumann, U. Discovery of cyclic sulfoxide hydroxyethylamines as potent and selective β-site APP-cleaving enzyme 1 (BACE1) inhibitors: structure based design and in vivo reduction of amyloid β-peptides. *Bioorg. Med. Chem. Lett.* **2013**, *23*, 5300−5306.
(35) Edwards, P. D.; Albert, J. S.; Sylvester, M.; Aharony, D.; Andisik, D.; Callaghan, O.; Campbell, J. B.; Carr, R. A.; Chessari, G.; Congreve, M.; Frederickson, M.; Folmer, R. H. A.; Geschwindner, S.; Koether, G.; Kolmodin, K.; Krumrine, J.; Mauger, R. C.; Murray, C. W.; Olsson, L.-L.; Patel, S.; Spear, N.; Tian, G. Application of fragment-based lead generation to the discovery of novel, cyclic amidine β-secretase inhibitors with nanomolar potency, cellular activity, and high ligand efficiency. *J. Med. Chem.* **2007**, *50*, 5912−5925.
(36) Malamas, M. S.; Erdei, J.; Gunawan, I.; Barnes, K.; Johnson, M.; Hui, Y.; Turner, J.; Hu, Y.; Wagner, E.; Fan, K.; Olland, A.; Bard, J.; Robichaud, A. J. Aminoimidazoles as potent and selective human beta-secretase (BACE1) inhibitors. *J. Med. Chem.* **2009**, *52*, 6314−6323.
(37) Kobayashi, N.; Ueda, K.; Itoh, N.; Suzuki, S.; Sakaguchi, G.; Kato, A.; Yukimasa, A.; Hori, A.; Koriyama, Y.; Haraguchi, H.; Yasui, K.; Kanda, Y. Preparation of 2-aminodihydrothiazine derivatives as β-secretase inhibitors. WO2007049532A1, 2007.
(38) Jennings, L. D.; Cole, D. C.; Stock, J. R.; Sukhdeo, M. N.; Ellingboe, J. W.; Cowling, R.; Jin, G.; Manas, E. S.; Fan, K. Y.; Malamas, M. S.; Harrison, B. L.; Jacobsen, S.; Chopra, R.; Lohse, P. A.; Moore, W. J.; O'Donnell, M. M.; Hu, Y.; Robichaud, A. J.; Turner, M. J.; Wagner, E.; Bard, J. Acylguanidine inhibitors of beta-secretase: optimization of the pyrrole ring substituents extending into the S1′ substrate binding pocket. *Bioorg. Med. Chem. Lett.* **2008**, *18*, 767−771.
(39) Oehlrich, D.; Prokopcova, H.; Gijsen, H. J. The evolution of amidine-based brain penetrant BACE1 inhibitors. *Bioorg. Med. Chem. Lett.* **2014**, *24*, 2033−2045.
(40) May, P. C.; Willis, B. A.; Lowe, S. L.; Dean, R. A.; Monk, S. A.; Cocke, P. J.; Audia, J. E.; Boggs, L. N.; Borders, A. R.; Brier, R. A.; Calligaro, D. O.; Day, T. A.; Ereshefsky, L.; Erickson, J. A.; Gevorkyan, H.; Gonzales, C. R.; James, D. E.; Jhee, S. S.; Komjathy, S. F.; Li, L.; Lindstrom, T. D.; Mathes, B. M.; Martenyi, F.; Sheehan, S. M.; Stout, S. L.; Timm, D. E.; Vaught, G. M.; Watson, B. M.; Winneroski, L. L.; Yang, Z.; Mergott, D. J. The potent BACE1 inhibitor LY2886721 elicits robust central Abeta pharmacodynamic responses in mice, dogs, and humans. *J. Neurosci.* **2015**, *35*, 1199−1210.
(41) May, P. C.; Dean, R. A.; Lowe, S. L.; Martenyi, F.; Sheehan, S. M.; Boggs, L. N.; Monk, S. A.; Mathes, B. M.; Mergott, D. J.; Watson, B. M.; Stout, S. L.; Timm, D. E.; Smith Labell, E.; Gonzales, C. R.;

https://doi.org/10.1021/acs.jmedchem.0c02143
J. Med. Chem. 2021, 64, 4677−4696

Nakano, M.; Jhee, S. S.; Yen, M.; Ereshefsky, L.; Lindstrom, T. D.; Calligaro, D. O.; Cocke, P. J.; Greg Hall, D.; Friedrich, S.; Citron, M.; Audia, J. E. Robust central reduction of amyloid-beta in humans with an orally available, non-peptidic beta-secretase inhibitor. *J. Neurosci.* **2011**, *31*, 16507−16516.

(42) Rombouts, F. J.; Tresadern, G.; Delgado, O.; Martinez-Lamenca, C.; Van Gool, M.; Garcia-Molina, A.; Alonso de Diego, S. A.; Oehlrich, D.; Prokopcova, H.; Alonso, J. M.; Austin, N.; Borghys, H.; Van Brandt, S.; Surkyn, M.; De Cleyn, M.; Vos, A.; Alexander, R.; Macdonald, G.; Moechars, D.; Gijsen, H.; Trabanco, A. A. 1,4-Oxazine beta-secretase 1 (BACE1) inhibitors: from hit generation to orally bioavailable brain penetrant leads. *J. Med. Chem.* **2015**, *58*, 8216−8235.

(43) Scott, J. D.; Li, S. W.; Brunskill, A. P.; Chen, X.; Cox, K.; Cumming, J. N.; Forman, M.; Gilbert, E. J.; Hodgson, R. A.; Hyde, L. A.; Jiang, Q.; Iserloh, U.; Kazakevich, I.; Kuvelkar, R.; Mei, H.; Meredith, J.; Misiaszek, J.; Orth, P.; Rossiter, L. M.; Slater, M.; Stone, J.; Strickland, C. O.; Voigt, J. H.; Wang, G.; Wang, H.; Wu, Y.; Greenlee, W. J.; Parker, E. M.; Kennedy, M. E.; Stamford, A. W. Discovery of the 3-imino-1,2,4-thiadiazinane 1,1-dioxide derivative verubecestat (MK-8931) - a beta-site amyloid precursor protein cleaving enzyme 1 inhibitor for the treatment of Alzheimer's disease. *J. Med. Chem.* **2016**, *59*, 10435−10450.

(44) Butler, C. R.; Brodney, M. A.; Beck, E. M.; Barreiro, G.; Nolan, C. E.; Pan, F.; Vajdos, F.; Parris, K.; Varghese, A. H.; Helal, C. J.; Lira, R.; Doran, S. D.; Riddell, D. R.; Buzon, L. M.; Dutra, J. K.; Martinez-Alsina, L. A.; Ogilvie, K.; Murray, J. C.; Young, J. M.; Atchison, K.; Robshaw, A.; Gonzales, C.; Wang, J.; Zhang, Y.; O'Neill, B. T. Discovery of a series of efficient, centrally efficacious BACE1 inhibitors through structure-based drug design. *J. Med. Chem.* **2015**, *58*, 2678−2702.

(45) Cheng, Y.; Brown, J.; Judd, T. C.; Lopez, P.; Qian, W.; Powers, T. S.; Chen, J. J.; Bartberger, M. D.; Chen, K.; Dunn, R. T., 2nd; Epstein, O.; Fremeau, R. T., Jr.; Harried, S.; Hickman, D.; Hitchcock, S. A.; Luo, Y.; Minatti, A. E.; Patel, V. F.; Vargas, H. M.; Wahl, R. C.; Weiss, M. M.; Wen, P. H.; White, R. D.; Whittington, D. A.; Zheng, X. M.; Wood, S. An orally available BACE1 inhibitor that affords robust CNS Abeta reduction without cardiovascular liabilities. *ACS Med. Chem. Lett.* **2015**, *6*, 210−215.

(46) Jeppsson, F.; Eketjall, S.; Janson, J.; Karlstrom, S.; Gustavsson, S.; Olsson, L. L.; Radesater, A. C.; Ploeger, B.; Cebers, G.; Kolmodin, K.; Swahn, B. M.; von Berg, S.; Bueters, T.; Falting, J. Discovery of AZD3839, a potent and selective BACE1 inhibitor clinical candidate for the treatment of Alzheimer disease. *J. Biol. Chem.* **2012**, *287*, 41245−41257.

(47) Schechter, I.; Berger, A. On the size of the active site in proteases. I. papain. *Biochem. Biophys. Res. Commun.* **1967**, *27*, 157−162.

(48) Wu, Y.-J.; Guernon, J.; Yang, F.; Snyder, L.; Shi, J.; McClure, A.; Rajamani, R.; Park, H.; Ng, A.; Lewis, H.; Chang, C. Y.; Camac, D.; Toyn, J. H.; Ahlijanian, M. K.; Albright, C. F.; Macor, J. E.; Thompson, L. A. Targeting the BACE1 active site flap leads to a potent inhibitor that elicits robust brain Aβ reduction in rodents. *ACS Med. Chem. Lett.* **2016**, *7*, 271−276.

(49) Woltering, T. J.; Wostl, W.; Hilpert, H.; Rogers-Evans, M.; Pinard, E.; Mayweg, A.; Gobel, M.; Banner, D. W.; Benz, J.; Travagli, M.; Pollastrini, M.; Marconi, G.; Gabellieri, E.; Guba, W.; Mauser, H.; Andreini, M.; Jacobsen, H.; Power, E.; Narquizian, R. BACE1 inhibitors: a head group scan on a series of amides. *Bioorg. Med. Chem. Lett.* **2013**, *23*, 4239−4243.

(50) Hilpert, H.; Guba, W.; Woltering, T. J.; Wostl, W.; Pinard, E.; Mauser, H.; Mayweg, A. V.; Rogers-Evans, M.; Humm, R.; Krummenacher, D.; Muser, T.; Schnider, C.; Jacobsen, H.; Ozmen, L.; Bergadano, A.; Banner, D. W.; Hochstrasser, R.; Kuglstatter, A.; David-Pierson, P.; Fischer, H.; Polara, A.; Narquizian, R. beta-Secretase (BACE1) inhibitors with high in vivo efficacy suitable for clinical evaluation in Alzheimer's disease. *J. Med. Chem.* **2013**, *56*, 3980−3995.

(51) Veenstra, S. J.; Rueeger, H.; Voegtle, M.; Lueoend, R.; Holzer, P.; Hurth, K.; Tintelnot-Blomley, M.; Frederiksen, M.; Rondeau, J. M.; Jacobson, L.; Staufenbiel, M.; Neumann, U.; Machauer, R. Discovery of amino-1,4-oxazines as potent BACE-1 inhibitors. *Bioorg. Med. Chem. Lett.* **2018**, *28*, 2195−2200.

(52) Morgenthaler, M.; Schweizer, E.; Hoffmann-Roder, A.; Benini, F.; Martin, R. E.; Jaeschke, G.; Wagner, B.; Fischer, H.; Bendels, S.; Zimmerli, D.; Schneider, J.; Diederich, F.; Kansy, M.; Muller, K. Predicting and tuning physicochemical properties in lead optimization: amine basicities. *ChemMedChem* **2007**, *2*, 1100−1115.

(53) Gijsen, H. J. M.; Alonso de Diego, S. A.; De Cleyn, M.; Garcia-Molina, A.; Macdonald, G. J.; Martinez-Lamenca, C.; Oehlrich, D.; Prokopcova, H.; Rombouts, F. J. R.; Surkyn, M.; Trabanco, A. A.; Van Brandt, S.; Van den Bossche, D.; Van Gool, M.; Austin, N.; Borghys, H.; Dhuyvetter, D.; Moechars, D. Optimization of 1,4-oxazine beta-secretase 1 (BACE1) inhibitors toward a clinical candidate. *J. Med. Chem.* **2018**, *61*, 5292−5303.

(54) Badiger, S.; Chebrolu, M.; Hurth, K.; Jacquier, S.; Lueoend, R. M.; Machauer, R.; Rueeger, H.; Tintelnot-Blomley, M.; Veenstra, S. J.; Voegtle, M. Novel heterocyclic derivatives as BACE inhibitors and their preparation and use in the treatment of neurological disorders. WO2012095469A1, 2012.

(55) Neumann, U.; Jacobson, L. H.; Perrot, L.; Beltz, K.; Vogg, B.; Brzak, I.; Tanja, D.; Trappe, V.; Kolly, C.; Frieauff, W.; Dubost, V.; Jivkov, M. N.; Theil, D.; Staufenbiel, M.; Shimshek, D. R. Preclinical pharmacology of BACE inhibitor CNP520. *Alzheimer's Dementia* **2016**, *12*, P433−P434.

(56) Curphey, T. J. Thionation with the reagent combination of phosphorus pentasulfide and hexamethyldisiloxane. *J. Org. Chem.* **2002**, *67*, 6461−6473.

(57) Moser, H.; Fliri, A.; Steiger, A.; Costello, G.; Schreiber, J.; Eschenmoser, A. Poly(dipeptamidinium)-Salze: Definition und Methoden zur präparativen Herstellung. *Helv. Chim. Acta* **1986**, *69*, 1224−1262.

(58) Shen, M.; Li, C. Asymmetric iodolactamization induced by chiral oxazolidine auxiliary. *J. Org. Chem.* **2004**, *69*, 7906−7909.

(59) Gataullin, R. R.; Afon'kin, I. S.; Fatykhov, A. A.; Spirikhin, L. V.; Abdrakhmanov, I. B. Iodocyclization of N-(2-nitrophenyl)- and N-phenyl-N′-[2-(alk-1-enyl)phenyl]ethanimidamides. *Mendeleev Commun.* **2001**, *11*, 201−202.

(60) Brauer, D. J.; Schenk, S.; Roßenbach, S.; Tepper, M.; Stelzer, O.; Häusler, T.; Sheldrick, W. S. Water soluble phosphines: part XIII. chiral phosphine ligands with amino acid moieties. *J. Organomet. Chem.* **2000**, *598*, 116−126.

(61) Huang, H.; La, D. S.; Cheng, A. C.; Whittington, D. A.; Patel, V. F.; Chen, K.; Dineen, T. A.; Epstein, O.; Graceffa, R.; Hickman, D.; Kiang, Y. H.; Louie, S.; Luo, Y.; Wahl, R. C.; Wen, P. H.; Wood, S.; Fremeau, R. T., Jr. Structure- and property-based design of aminooxazoline xanthenes as selective, orally efficacious, and CNS penetrable BACE inhibitors for the treatment of Alzheimer's disease. *J. Med. Chem.* **2012**, *55*, 9156−9169.

(62) Box, K.; Bevan, C.; Comer, J.; Hill, A.; Allen, R.; Reynolds, D. High-throughput measurement of pKa values in a mixed-buffer linear pH gradient system. *Anal. Chem.* **2003**, *75*, 883−892.

(63) Neumann, U.; Rueeger, H.; Machauer, R.; Veenstra, S. J.; Lueoend, R. M.; Tintelnot-Blomley, M.; Laue, G.; Beltz, K.; Vogg, B.; Schmid, P.; Frieauff, W.; Shimshek, D. R.; Staufenbiel, M.; Jacobson, L. H. A novel BACE inhibitor NB-360 shows a superior pharmacological profile and robust reduction of amyloid-beta and neuroinflammation in APP transgenic mice. *Mol. Neurodegener.* **2015**, *10*, No. 44.

(64) Rochin, L.; Hurbain, I.; Serneels, L.; Fort, C.; Watt, B.; Leblanc, P.; Marks, M. S.; De Strooper, B.; Raposo, G.; van Niel, G. BACE2 processes PMEL to form the melanosome amyloid matrix in pigment cells. *Proc. Natl. Acad. Sci. U.S.A.* **2013**, *110*, 10658−10663.

(65) Shimshek, D. R.; Jacobson, L. H.; Kolly, C.; Zamurovic, N.; Balavenkatraman, K. K.; Morawiec, L.; Kreutzer, R.; Schelle, J.; Jucker, M.; Bertschi, B.; Theil, D.; Heier, A.; Bigot, K.; Beltz, K.; Machauer, R.; Brzak, I.; Perrot, L.; Neumann, U. Pharmacological BACE1 and

https://doi.org/10.1021/acs.jmedchem.0c02143
J. Med. Chem. 2021, 64, 4677−4696

BACE2 inhibition induces hair depigmentation by inhibiting PMEL17 processing in mice. *Sci. Rep.* **2016**, *6*, No. 21917.
(66) Beckmann, N.; Doelemeyer, A.; Zurbrugg, S.; Bigot, K.; Theil, D.; Frieauff, W.; Kolly, C.; Moulin, P.; Neddermann, D.; Kreutzer, R.; Perrot, L.; Brzak, I.; Jacobson, L. H.; Staufenbiel, M.; Neumann, U.; Shimshek, D. R. Longitudinal noninvasive magnetic resonance imaging of brain microhemorrhages in BACE inhibitor-treated APP transgenic mice. *Neurobiol. Aging* **2016**, *45*, 50−60.
(67) Schelle, J.; Hasler, L. M.; Gopfert, J. C.; Joos, T. O.; Vanderstichele, H.; Stoops, E.; Mandelkow, E. M.; Neumann, U.; Shimshek, D. R.; Staufenbiel, M.; Jucker, M.; Kaeser, S. A. Prevention of tau increase in cerebrospinal fluid of APP transgenic mice suggests downstream effect of BACE1 inhibition. *Alzheimer's Dementia* **2017**, *13*, 701−709.
(68) Bacioglu, M.; Maia, L. F.; Preische, O.; Schelle, J.; Apel, A.; Kaeser, S. A.; Schweighauser, M.; Eninger, T.; Lambert, M.; Pilotto, A.; Shimshek, D. R.; Neumann, U.; Kahle, P. J.; Staufenbiel, M.; Neumann, M.; Maetzler, W.; Kuhle, J.; Jucker, M. Neurofilament light chain in blood and CSF as marker of disease progression in mouse models and in neurodegenerative diseases. *Neuron* **2016**, *91*, 56−66.
(69) Schelle, J.; Wegenast-Braun, B. M.; Fritschi, S. K.; Kaeser, S. A.; Jährling, N.; Eicke, D.; Skodras, A.; Beschorner, N.; Obermueller, U.; Häsler, L. M.; Wolfer, D. P.; Mueggler, T.; Shimshek, D. R.; Neumann, U.; Dodt, H. U.; Staufenbiel, M.; Jucker, M. Early Aβ reduction prevents progression of cerebral amyloid angiopathy. *Ann. Neurol.* **2019**, *86*, 561−571.
(70) Esterházy, D.; Stutzer, I.; Wang, H.; Rechsteiner, M. P.; Beauchamp, J.; Dobeli, H.; Hilpert, H.; Matile, H.; Prummer, M.; Schmidt, A.; Lieske, N.; Boehm, B.; Marselli, L.; Bosco, D.; Kerr-Conte, J.; Aebersold, R.; Spinas, G. A.; Moch, H.; Migliorini, C.; Stoffel, M. Bace2 is a beta cell-enriched protease that regulates pancreatic beta cell function and mass. *Cell Metab.* **2011**, *14*, 365−377.
(71) Matafora, V.; Farris, F.; Restuccia, U.; Tamburri, S.; Martano, G.; Bernardelli, C.; Sofia, A.; Pisati, F.; Casagrande, F.; Lazzari, L.; Marsoni, S.; Bonoldi, E.; Bachi, A. Amyloid aggregates accumulate in melanoma metastasis modulating YAP activity. *EMBO Rep.* **2020**, *21*, No. e50446.
(72) Neumann, U.; Ufer, M.; Jacobson, L. H.; Rouzade-Dominguez, M. L.; Huledal, G.; Kolly, C.; Lüönd, R. M.; Machauer, R.; Veenstra, S. J.; Hurth, K.; Rueeger, H.; Tintelnot-Blomley, M.; Staufenbiel, M.; Shimshek, D. R.; Perrot, L.; Frieauff, W.; Dubost, V.; Schiller, H.; Vogg, B.; Beltz, K.; Avrameas, A.; Kretz, S.; Pezous, N.; Rondeau, J. M.; Beckmann, N.; Hartmann, A.; Vormfelde, S.; David, O. J.; Galli, B.; Ramos, R.; Graf, A.; Lopez Lopez, C. The BACE-1 inhibitor CNP520 for prevention trials in Alzheimer's disease. *EMBO Mol. Med.* **2018**, *10*, No. e9316.
(73) Zhu, K.; Xiang, X.; Filser, S.; Marinkovic, P.; Dorostkar, M. M.; Crux, S.; Neumann, U.; Shimshek, D. R.; Rammes, G.; Haass, C.; Lichtenthaler, S. F.; Gunnersen, J. M.; Herms, J. Beta-site amyloid precursor protein cleaving enzyme 1 inhibition impairs synaptic plasticity via seizure protein 6. *Biol. Psychiatry* **2018**, *83*, 428−437.
(74) Neumann, U.; Machauer, R.; Shimshek, D. R. The β-secretase (BACE) inhibitor NB-360 in preclinical models: from amyloid-β reduction to downstream disease-relevant effects. *Br. J. Pharmacol.* **2019**, *176*, 3435−3446.
(75) Wohnsland, F.; Faller, B. High-throughput permeability pH profile and high-throughput alkane/water log P with artificial membranes. *J. Med. Chem.* **2001**, *44*, 923−930.
(76) Hanessian, S.; Yun, H.; Hou, Y.; Yang, G.; Bayrakdarian, M.; Therrien, E.; Moitessier, N.; Roggo, S.; Veenstra, S.; Tintelnot-Blomley, M.; Rondeau, J. M.; Ostermeier, C.; Strauss, A.; Ramage, P.; Paganetti, P.; Neumann, U.; Betschart, C. Structure-based design, synthesis, and memapsin 2 (BACE) inhibitory activity of carbocyclic and heterocyclic peptidomimetics. *J. Med. Chem.* **2005**, *48*, 5175−5190.
(77) Kabsch, W. Automatic processing of rotation diffraction data from crystals of initially unknown symmetry and cell constants. *J. Appl. Crystallogr.* **1993**, *26*, 795−800.
(78) Kroemer, M.; Dreyer, M. K.; Wendt, K. U. APRV - a program for automated data processing, refinement and visualization. *Acta Crystallogr. D Biol. Crystallogr.* **2004**, *60*, 1679−1682.
(79) Brünger, A. T.; Adams, P. D.; Clore, G. M.; DeLano, W. L.; Gros, P.; Grosse-Kunstleve, R. W.; Jiang, J. S.; Kuszewski, J.; Nilges, M.; Pannu, N. S.; Read, R. J.; Rice, L. M.; Simonson, T.; Warren, G. L. Crystallography & NMR system: A new software suite for macromolecular structure determination. *Acta Crystallogr., Sect. D: Biol. Crystallogr.* **1998**, *54*, 905−921.
(80) Emsley, P.; Lohkamp, B.; Scott, W. G.; Cowtan, K. Features and development of Coot. *Acta Crystallogr. D Biol. Crystallogr.* **2010**, *66*, 486−501.

https://doi.org/10.1021/acs.jmedchem.0c02143
J. Med. Chem. 2021, 64, 4677−4696